書籍

著者氏名	論文タイトル名	書籍全体の編集者名	書　籍　名	出版社名	出版地	出版年	ページ

雑誌

発表者氏名	論文タイトル名	発表誌名	巻号	ページ	出版年
Tomono S., Miyoshi N., Ohshisma H.	Comprehensive analysis of the lipophilic reactive carbonyls present in biological specimens by LC/ESI-MS/MS	J Chromatogr B Analyt Technol Biomed Life Sci	988	149-156	2015
Futakuchi M, Fukamachi K, Suzui M.	IHeterogeneity of tumor cells in the bone microenvironment: mechanisms and therapeutic targets for bone metastasis of prostate or breast cancer.	Adv Drug Deliv Rev.	99	206-211	2015
Tuboly E, Futakuchi M, Varga G, Erces D, Tokes T, Meszaros A, Kaszaki J, Suzui M, Imai M, Okad	C5a inhibitor protects ischemia/reperfusion injury in rat small intestine. Microbiol Immunol,	Microbiol Immunol	60	35-46	2015
Shibata K, Fukamachi K, Tsuji A, Saga T, Futakuchi M, Nagino M, Tsuda H, Suzui M.	*In vivo* ^{18}F-fluorodeoxyglucose-positron emission tomography/computed tomography imaging of pancreatic tumors in a transgenic rat model carrying the human *Kras*^{G12V} oncogene.	Oncol Lett.	9	2112-2118	2015
Suzui M, Futakuchi M., Fukamachi K., Numano T., Mohamed Abd Elgied, Takahashi S., Ohnishi M., Omori, T., Tsuruoka S., Hirose A., Kanno J., Sakamoto Y., Alexander D.B., Alexander W.T., Xu J, Tsuda H.	Multiwalled carbon nanotubes intratracheally instilled into the rat lung induce malignant mesothelioma and lung tumors.	Cancer Science		in press	2016
Xu J., Alexander D.B., Iigo M., Hamano H., Takahashi S., Yokoyama T., Kato M., Usami I., Tokuyama T., Tsutsumi M., Tamura M., Oguri T., Niimi A., Hayashi Y., Yokoyama Y.,Tonegawa K., Fukamachi K., Futakuchi M., Sakai Y., Suzui M., Kamijima M., Hisanaga N., Omori	Chemokine (C-C motif) ligand 3 detection in the serum of persons exposed to asbestos: A patient-based study.	Cancer Science	106	825-832	2015

Xu J, Alexander D. B., Futakuchi M., Numano T., Fukamachi K., Suzui M., Omori T., Kanno J., Hirose A., Tsuda H.	Size- and shape-dependent pleural translocation,deposition, fibrogenesis, and mesothelial proliferation by multiwalled carbon nanotubes.	Cancer Science	105	763-769	2014

Ⅳ．研究成果の刊行物・別冊

Journal of Chromatography B, 988 (2015) 149–156

Contents lists available at ScienceDirect

Journal of Chromatography B

journal homepage: www.elsevier.com/locate/chromb

Comprehensive analysis of the lipophilic reactive carbonyls present in biological specimens by LC/ESI-MS/MS

Susumu Tomono*, Noriyuki Miyoshi, Hiroshi Ohshima

Laboratory of Longevity Biochemistry, Graduate School of Integrated Pharmaceutical and Nutritional Sciences, Graduate Program in Food and Nutritional Sciences, University of Shizuoka, Shizuoka 422-8526, Japan

ARTICLE INFO

Article history:
Received 6 September 2014
Accepted 25 February 2015
Available online 2 March 2015

Keywords:
Reactive carbonyl
Aldehyde
Dansyl hydrazine
LC/ESI-MS/MS
SRM
Lipid peroxidation

ABSTRACT

A new analytical method has been developed for profiling lipophilic reactive carbonyls (RCs) such as aldehydes and ketones in biological samples using liquid chromatography/electrospray ionization tandem mass spectrometry (LC/ESI-MS/MS) with selected reaction monitoring (SRM). The method consists of several phases, including (1) extraction of lipophilic RCs with a chloroform/methanol mixture; (2) derivatization of the extracted RCs with dansyl hydrazine (DH); and (3) SRM detection of the characteristic product ion of the 5-dimethylaminonaphthalene-1-sulfonyl moiety (*m/z* 236.1). The analytical results were expressed as RC maps, which allowed for the occurrence and levels of different lipophilic RCs to be visualized. We also developed a highly reproducible and accurate method to extract, purify and derivatize RCs in small volumes of biological specimens. This method was applied to the detection of free RCs in mice plasma samples, and resulted in the detection of more than 400 RCs in samples obtained from C57BL/6J mice. Thirty-four of these RCs were identified by comparison with authentic RCs. This method could be used to investigate the levels of RCs in biological and environmental samples, as well as studying the role of lipid peroxidation in oxidative stress related-disorders and discovering new biomarkers for the early diagnosis of these diseases.

1. Introduction

A wide variety of aldehydes and ketones (i.e., reactive carbonyls; RCs) can be found in human tissues and the environment, and these compounds are generally formed by the lipid peroxidation (LPO) of phospholipids (PLs), triacylglycerols (TGs), cholesterol and cholesteryl esters. For example, polyunsaturated fatty acids (PUFAs), which can be used to form PLs or TGs, can be oxidized to form lipid hydroperoxides [1], which can subsequently decompose to give a variety of different RCs, including alkanals, alkenals, 4-hydroxyalkenals and alkadienals [2–4]. RCs react with the amino groups in proteins, amino acids, nucleic acids, and PLs such as phosphatidylethanolamine and phosphatidylserine, to give the corresponding Schiff base adducts [4–8]. α,β-Unsaturated aldehydes, in particular, are highly reactive and readily undergo Michael addition reactions with amino and thiol groups to give the corresponding 1,4-addition products [9,10]. Increased levels of RCs such as acrolein, 4-hydroxy-2-nonenal (HNE) and malondialdehyde in human tissues have therefore been associated with elevated risks of cardiovascular disease and cancer, as well as several other chronic diseases, because they can react directly with proteins and nucleic acids and have an adverse impact on their structure, function and overall utility [4,5,11,12]. However, information pertaining to the occurrence and levels of various RCs in complicated biological specimens, as well as our general knowledge and understanding of their roles in diseases, remains limited.

A broad range of different analytical methods has been reported for investigating RCs. For example, the physiological and pathological levels of RCs can be analyzed by GC/MS following the conversion of the RCs to the corresponding *O*-pentafluorobenzyl-oxime (PFB-oxime) derivatives, and the subsequent conversion of the hydroxy moieties in the resulting oximes to the trimethylsilyl (TMS) ether derivatives [13]. 2,4-Dinitrophenylhydrazine (DNPH) has also been used to derivatize the RCs present in a variety of biological and environmental samples. The DNPH derivatives can be analyzed by HPLC

Abbreviations: AA, arachidonic acid; DH, dansyl hydrazine; DHA, docosahexaenoic acid; 2,4-DDE, 2,4-decadienal; EDE, 4,5-epoxy-2-decenal; 2,4-HxDE, 2,4-hexadienal; 2,4-HpDE, 2,4-heptadienal; HNE, 4-hydroxy-2-nonenal; IS, internal standard; LA, linoleic acid; LC/ESI-MS/MS, liquid chromatography/electrospray ionization tandem mass spectrometry; LPO, lipid peroxidation; 2,4-NDE, 2,4-nonadienal; ONE, 4-oxo-2-nonenal; PLs, phospholipids; PUFAs, polyunsaturated fatty acids; RCs, reactive carbonyls; RSD, relative standard deviation; SRM, selected reaction monitoring; TGs, triacylglycerols.

* Corresponding author. Tel.: +81 54 264 5531; fax: +81 54 264 5530.
E-mail address: gp1535@u-shizuoka-ken.ac.jp (S. Tomono).

http://dx.doi.org/10.1016/j.jchromb.2015.02.036
1570-0232/

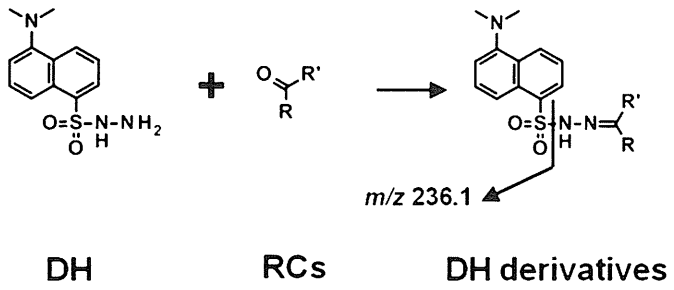

Fig. 1. Chemical structures of the RCs derivatized with DH, and the product ion with an *m/z* value of 236.1 formed by CID.

with UV detection or LC/MS [14,15]. Unfortunately, however, these methods lack the sensitivity and specificity required for the comprehensive analysis of trace amounts of the different RCs present in complicated biological and environmental samples.

Dansyl hydrazine (DH) is a fluorescent derivatization reagent that has been used for fluorescence detection as well as enhancing the ionization characteristics of aldehydes and ketones [16–18]. There are several advantages associated with the use of DH over other derivatizing agents. Most notably, the dimethylamino group of DH can be readily protonated under acidic conditions [19], and the resulting positively ionized DH derivatives can generate a product ion with an *m/z* value of 236.1 by collision-induced dissociation (CID). The detection of a product ion with an *m/z* value of 236.1 is therefore consistent with the formation of a 5-dimethylaminonaphthalene-1-sulfonyl moiety from the cleavage of the parent DH derivative (Fig. 1). Furthermore, the product ion spectra of the DH derivatives of RCs are generally simple and clear.

The aim of the current study was to develop a sensitive and specific method for the simultaneous detection of numerous lipophilic RCs using DH as a derivatizing agent. Verification experiments revealed that the product ion for the 5-dimethylaminonaphthalene-1-sulfonyl moiety (*m/z* 236.1) generated from the positively ionized RC-DH derivatives during the CID process could be measured over specific transition ranges. In this way, the mass spectral data could be used to provide unique signatures for the different RCs present in biological samples. The presence and quantity of various RCs in the different samples could then be compared by creating "RC maps" that consisted of the LC/MS retention times, *m/z* values, and relative peak intensities of the potential RCs. This approach allowed for the comprehensive detection of a variety of different RCs over a wide range of molecular weights, including those with unknown structures. Furthermore, this method was found to be highly sensitive and repeatable for the measurement of a range of RCs, as well as being applicable to different biological and environmental samples. This newly developed method was also validated for the quantification of free RCs present in the plasma of C57BL/6J mice.

2. Material and methods

2.1. Materials

Dansyl hydrazine (DH) was purchased from Invitrogen (Carlsbad, CA, USA). *p*-Toluenesulfonic acid (*p*-TsOH) and the RCs, including propanal, pentanal, butanal, 2-hexenal, hexanal, 2-heptenal, heptanal, octanal, 2-nonenal, nonanal, decanal, undecanal, dodecanal and tridecanal, were obtained from Sigma–Aldrich (St. Louis, MO, USA). Glyoxal, crotonaldehyde, 2,4-nonadienal (NDE), 2,4-decadienal (DDE), heptadecanal, hexadecanal, octadecanal, pentadecanal and tetradecanal were purchased from Tokyo Chemical Industry (Tokyo, Japan). 4-Hydroxy-2-hexenal (HHE), 4-hydroxy-2-nonenal (HNE), 4-oxo-2-nonenal (ONE) and 4,5-epoxy-2-decenal (EDE) were purchased from Cayman Chemical Company (Ann Arbor, MI, USA). *p*-Benzyloxybenzaldehyde (*p*-BOBA) and all of the other chemicals used in the current study were purchased from Wako Pure Chemical Industries (Osaka, Japan). Secosterols A and B were synthesized according to the procedure reported by Wentworth et al. [20], and their purities were verified by TLC and ^{1}H NMR analyses. Stock solutions of the RCs and an internal standard (IS) (*p*-BOBA 10 μM) were prepared separately in acetonitrile and stored at −20 °C prior to their use.

2.2. Profiling of the RCs in plasma

Frozen mouse plasma samples (stored −80 °C) were thawed on ice to 0 °C. Immediately after being thawed, a portion of the plasma sample (20 μL) was added to a solution consisting of 80 μL of distilled water, 2 μL of 10 μM IS (*p*-BOBA) and 200 μL of a mixture of chloroform/methanol (2:1, v/v), and the resulting mixture was vigorously agitated for 1 min. The mixture was then centrifuged at 15,000 rpm for 10 min and the organic phase was collected. The remaining precipitate and aqueous phase were then mixed with 200 μL of a mixture of chloroform/methanol (2:1, v/v), and the resulting mixture was centrifuged at 15,000 rpm for 10 min to give the organic phase. The combined organic phases were then subjected to a derivatization reaction with DH according to the procedure described below.

2.3. DH derivatization

The samples were mixed with 100 μL of acetonitrile containing 50 μg of DH and 10 μg of *p*-TsOH, and the resulting mixtures were incubated for 4 h at ambient temperature in the absence of light. The mixtures were then evaporated to dryness in vacuo to give the corresponding derivatized residues, which were individually dissolved in 200 μL of acetonitrile. Aliquots (5 μL) of these stock solutions were analyzed seven times by LC/ESI-MS/MS as described below.

2.4. LC/ESI-MS/MS

The LC/ESI-MS/MS analyses were performed on an Agilent 1200 series HPLC system (Agilent Technologies, Santa Clara, CA, USA) using a TSKgel Super-Octyl column (2.3 μm, 100 mm × 2.0 mm, TOSOH, Tokyo, Japan) and an Agilent G6410B triple quadrupole tandem mass spectrometer with an electrospray ionization device running in the positive ion mode. The detector conditions were as follows: capillary voltage at 4000 V, source temperature of 300 °C, drying gas flow rate of 7 L/min, nebulizer gas at 20 psi, fragmentor at 200 V and collision energies of 13 eV (*m/z* 275–349), 20 eV (*m/z* 350–449) and 29 eV (*m/z* 450–949). Nitrogen was used as the collision gas. The RC-DH derivatives were detected using the selected reaction monitoring (SRM) mode. This strategy was designed to detect a specific product ion with an *m/z* value of 236.1 by CID. This product ion was assigned to the 5-dimethylaminonaphthalene-1-sulfonyl moiety derived from the positively ionized DH derivatives. The RC-DH derivatives were therefore detected with high sensitivity by monitoring their transmitting $[M+H]^+ \rightarrow 236.1$ transitions (Fig. 1). A total of 675 SRM transitions were monitored for each DH-derivatized sample, with the transitions ranging from *m/z* 275 → 236.1 to 949 → 236.1, and a total of 100 channels were monitored simultaneously for each sample injection. One channel from each injection was reserved for monitoring the transition of *p*-BOBA-DH (IS) at *m/z* 460 → 236.1. Each sample was injected seven times to complete the monitoring of the 675 SRM transitions.

In order to verify whether the peaks of DH-derivatives were derived from aldehydes, ketones or other artifacts, mixtures of standard RCs or mice plasma samples were reduced by treatment

for 1 h at 37 °C with 0.1 M sodium borohydride ($NaBH_4$). $NaBH_4$ can convert aldehydes and ketones to corresponding primary and secondary alcohols, which are not derivatized with DH. After the reduction of standard RCs or mice plasma samples with $NaBH_4$, the peaks corresponding to DH-RCs were not detected by LC/ESI-MS/MS (SRM) except for those which were derived from DH reagents (data not shown). Some of the solvents used in this study were found to be contaminated with RCs. Therefore, it was necessary to calculate the amounts of RCs by subtracting the redundant (background) peaks such as the spike noises and artifactual DH derivatives derived from solvents and reagents.

In terms of the mobile phases used for the LC/ESI-MS/MS analyses, solvent A consisted of a 0.1% (v/v) solution of formic acid in water, whereas solvent B consisted of a 0.1% (v/v) solution of formic acid in acetonitrile. The DH derivatives were eluted from the column using a linear gradient, which started at 80% solvent A and 20% solvent B, and progressed to 100% solvent B over a period of 10 min. The system was then eluted with 100% solvent B for 10 min before being returned to the initial conditions over a period of 10 min to allow for the equilibration of the column. The system was operated at a constant flow rate of 0.2 mL/min for all of the analyses.

2.5. Stabilities of RCs during storage

Plasma samples were obtained from five 10-week-old male C57BL/6J mice (body weight ~27 g). The plasma samples (100 μL) were spiked with five representative RCs, including 4-hydroxy-2-alkenal (HNE), 2-alkenal (2-hexenal) and 2,4-alkadienal (2,4-NDE), as well as a short chain alkanal (hexanal) (5 pmol each) and a long chain alkanal (hexadecanal) (100 pmol). The spiked samples were then stored on ice for 0–60 min or stored at −80 °C for 4 weeks.

2.6. LOD and LOQ

The limit of detection (LOD) was defined as the calculated concentration at a signal to noise ratio of ≥5 (S/N = 5). The limit of quantification (LOQ) was based on a signal to noise ratio of ≥10 and validated at a concentration measured with an RSD ≤20%.

2.7. Recovery

The plasma samples (20 μL) were spiked or left unspiked (control) with a mixture containing several RC standards at 2 or 10 pmol. The samples were then extracted with a chloroform/methanol (2:1, v/v) mixture and the organic phases were analyzed according to the procedure described above. The estimated recoveries were calculated as follows:

Recovery = [(concentrations of extracted total RCs − concentrations of extracted endogenous RCs)/concentrations of spiked RCs standards] × 100 (%)

2.8. Calibration curves for RCs

Calibration and validation studies were conducted involving the addition of several different RCs to the mice plasma. Varying amounts of the RCs (i.e., 0.1, 0.2, 0.5, 1, 2, 5, 10, 20, 50 and 100 pmol for each RC species) and a fixed amount of the IS (20 pmol) were spiked into the mouse plasma (20 μL), and the resulting mixtures were extracted, derivatized and subjected to LC/ESI-MS/MS analysis. Calibration curves were constructed by plotting the peak area ratios [i.e., (total RCs − endogenous RCs)/IS against the concentration of RCs]. All of the determinations at the different concentrations were performed in triplicate.

2.9. Assay precision and accuracy (analytical recovery)

The accuracy and precision levels of the assay were determined based on intra- and inter-day variations in the results obtained using the method described above.

Plasma samples (20 μL) were spiked with RCs at concentrations of 0, 50, 100, 500 and 1000 pmol/mL, respectively, $n = 3$. IS (20 pmol) was then added to each sample, and the resulting mixtures were extracted, derivatized and analyzed by LC/ESI-MS/MS. The intra-day precision values for the different concentrations were also calculated from determination experiments, which were conducted in triplicate. The inter-day precision was evaluated by analyzing the same sample over a 5-day period, and the precision was determined as the relative standard deviation (RSD, %). The accuracies (analytical recoveries) of the RCs were defined as the total concentration of RCs in the spiked samples/(the concentration of RCs detected in the unspiked samples + the spiked concentration) × 100 (%).

3. Results and discussion

3.1. RCs derivatization with DH

We initially derivatized 36 authentic RCs with DH and analyzed the resulting products by LC/ESI-MS/MS. All of the derivatized RCs gave the corresponding $[M+H]^+$ mass ions, as well as the common product ion with an *m/z* value of 236.1, which was assigned to the 5-dimethylaminonaphthalene-1-sulfonyl moiety generated from the cleavage of the DH derivatives during CID (Fig. 1). On the basis of these results, we developed a global analytical method for the comprehensive profiling of the lipophilic RCs present in biological samples using LC/ESI-MS/MS with SRM. The SRM assay was designed to detect the characteristic product ion with an *m/z* value of 236.1, which was derived from the positively ionized RC-DH derivatives transmitting the $[M+H]^+ \rightarrow 236.1$ transition over 675 SRM transitions, ranging from transitions of *m/z* 275 → 236.1 to 949 → 236.1. For each sample injection, a total of 100 channels were monitored simultaneously. We compared the sensitivities (S/N ratio) of LC/MS detection by SRM and precursor ion scan (PIS) of DH-RC standards (Supplementary Table 1). The sensitivities of SRM were 1.6- to 110-fold better than the PIS. These results indicate that the SRM can be used for the sensitive detection of various RCs by MS.

Supplementary Table 1 can be found, in the online version, at http://dx.doi.org/10.1016/j.jchromb.2015.02.036.

Typical SRM chromatograms for the DH-derivatives of the 36 RCs and IS (*p*-BOBA) are shown in Fig. 2. These results effectively confirmed that the developed SRM assay could be used detect all of the RCs tested in the current study, with the RCs giving the corresponding $[M+H]^+$ ions as well as the common product ion of the 5-dimethylaminonaphthalene-1-sulfonyl moiety by CID. Although 4-hydroxy-2-alkenals such as HNE and HHE possess a chiral center at their C4 position, the *syn*- and *anti*-isomers of their DH derivatives could not be separated in this condition, and it was therefore not possible to detect the different isomers as single peaks. Furthermore, despite using an excess of DH, dicarbonyl compounds such as glyoxal and ONE only reacted to give the mono-DH derivatives under the current derivatization conditions. Ions corresponding to bis-DH derivatives were therefore not observed under these SRM conditions (data not shown).

3.2. Validation of the proposed method using biological samples

This method was validated based on the recovery data and calibration curves of the different RCs that had been spiked into the

Table 1
Linearity, limit of detection (LOD), limit of quantification (LOQ) and recovery values of the LC/ESI-MS/MS assay for the RCs.

Compounds	MW (intact)	$[M+H]^+$ (DH derivatives)	t_R (min)	LOD (fmol)[a]	LOQ (fmol)[b]	Calibration range (fmol)	Linear equation	Linearity (r^2)	Recovery (%)[c]
p-BOBA (IS)	212.21	460	11.8	1	1	–	–	–	101.4
Acrolein	56.06	304	9.3	1	2.5	25–1000	$y=0.0004x+0.0052$	0.9996	95.5
Glyoxal	58.04	306	8.4	20	50	50–2500	$y=0.0014x+0.0872$	0.9991	100.3[d]
Propanal	58.08	306	9.3	10	25	25–1000	$y=0.0008x-0.0043$	0.9978	70.3
Crotonaldehyde	70.09	318	9.8	1	2.5	5–250	$y=0.0018x+0.0015$	0.9996	93.8
Butanal	72.11	320	10.1	1	2.5	25–1000	$y=0.0008x+0.0245$	0.992	88.4
Pentanal	86.13	334	10.8	10	25	25–1000	$y=0.0012x+0.0107$	0.9986	86.0
2,4-HxDE	96.14	344	10.8	1	2.5	5–250	$y=0.0024x+0.0224$	0.9944	82.1
2-Hexenal	98.14	346	11.1	1	2.5	5–250	$y=0.0027x-0.002$	0.9999	91.4
Hexanal	100.16	348	11.3	10	25	25–1000	$y=0.0024x+0.0211$	0.999	93.5
2,4-HpDE	110.17	358	11.2	1	2.5	5–250	$y=0.0021x+0.015$	0.995	83.6
2-Heptenal	112.17	360	11.6	1	2.5	5–250	$y=0.0003x-0.0009$	0.9997	89.8
HHE	114.14	362	8.9	1	2.5	5–250	$y=0.0008x-0.0021$	0.9998	92.5
Heptanal	114.18	362	11.8	10	25	25–1000	$y=0.0022x+0.0059$	0.9996	82.5
2-Octenal	126.2	374	12.0	1	2.5	5–250	$y=0.0139x+0.103$	0.9952	94.2
Octanal	128.21	376	12.2	10	25	50–2500	$y=0.0034x-0.1748$	0.9994	111.8[d]
2,4-NDE	138.22	386	12.1	1	2.5	5–250	$y=0.0041x+0.0259$	0.9962	73.6
2-Nonenal	140.22	388	12.4	1	2.5	5–250	y-0.0046$x-0.0051$	1	89.6
Nonanal	142.24	390	12.6	20	50	50–2500	$y=0.0028x-0.3148$	0.9977	89.0[d]
2,4-DDE	152.21	400	12.5	1	2.5	5–250	$y=0.0032x+0.0225$	0.9951	84.6
HNE	156.22	404	10.8	1	2.5	5–250	$y=0.0006x-0.0029$	0.9999	93.7
Decanal	156.27	404	13.0	20	50	50–2500	$y=0.004x-0.8092$	0.9971	94.6[d]
EDE	168.23	416	11.3	1	2.5	5–250	$y=0.0023x-0.0075$	0.9998	86.6
2-Undecenal	168.28	416	13.1	1	2.5	5–250	$y=0.0153x+0.0599$	0.9932	88.9
Undecanal	170.29	418	13.3	10	25	25–1000	$y=0.0004x-0.1044$	0.9986	92.0
Dodecanal	184.32	432	13.6	20	50	50–2500	$y=0.0039x-0.0099$	0.9983	83.2[d]
Tridecanal	198.34	446	13.9	10	25	25–1000	$y=0.0025x-0.0013$	0.9995	76.6
Tetradecanal	212.37	460	14.3	10	25	50–2500	$y=0.0055x-0.1422$	0.9989	81.2[d]
Pentadecanal	226.4	474	14.6	10	25	25–1000	$y=0.0013x+0.0051$	0.9997	84.8
Hexadecanal	240.43	488	14.8	10	25	50–2500	$y=0.0029x+0.0112$	0.9999	82.8[d]
Heptadecanal	254.45	502	15.1	1	2.5	5–250	$y=0.002x-0.0056$	0.9982	85.7
Octadecanal	268.48	516	15.4	10	25	50–2500	$y=0.0012x+0.074$	0.9964	80.1[d]
Secosterol-A	418.34	666	14.4	1	2.5	5–250	$y=0.0008x-0.0006$	0.9994	99.3
Secosterol-B	418.34	666	14.8	1	2.5	5–250	$y=0.0002x-0.0002$	0.9998	77.3

[a] These values were estimated at a S/N ratio of 5.
[b] These values were estimated at a S/N ratio of 10.
[c] $n=5$, spiked 2 pmol or [d]10 pmol.

C57BL/6J mice plasma samples (Table 1). Overall, this method was found to be sensitive, reproducible, accurate and specific for the RCs tested in the current study.

The stability properties of the some typical RCs (i.e., 2-hexenal, hexanal, 2,4-NDE, HNE and hexadecanal) that had been added to the mice plasma were determined experimentally (Fig. 3A, B, Supplementary Fig. 1). Samples of the mouse plasma were spiked with 5 or 100 pmol of specific RCs, and the resulting mixtures were kept on ice for 60 min. Subsequent analysis revealed that almost all of the α,β-unsaturated RCs tested (i.e., 2-hexenal and HNE) disappeared rapidly, whereas the other RCs tested (i.e., hexanal, 2,4-NDE and hexadecanal) disappeared at a much slower rate, with about half of the amounts added remained after an incubation period of 60 min on ice (Fig. 3A). On the other hand, Fig. 3B shows that there were no significant differences between the recoveries of the RCs added to the mouse plasma before and after the samples had been stored 4 weeks at −80 °C. These results suggest that it is necessary to extract the RCs as quickly as possible following thawing of frozen plasma samples to obtain their high recoveries. In addition, in order to analyze unstable aldehydes more accurately, new methods, for example adding stable isotope-labeled aldehydes as IS immediately after sampling, may be further developed and validated. The RCs appeared to react with glutathione or the amino groups of the proteins, amino acids, nucleic acids, and PLs, such as phosphatidylethanolamine and phosphatidylserine, to give the corresponding Schiff base adducts [4–8]. α,β-Unsaturated aldehydes, in particular, are highly reactive and readily undergo Michael addition reactions with amino and thiol groups to give the corresponding 1,4-addition products [9,10]. Compounds of this type can also be metabolized enzymatically into other compounds. For these reasons, in order to evaluate the occurrence and biological reactivities of α,β-unsaturated aldehydes, methods to analyze their adducts with amino acids, proteins, DNA and PLs in biological samples should be further developed.

Supplementary Fig. 1 can be found, in the online version, at http://dx.doi.org/10.1016/j.jchromb.2015.02.036.

Based on the stability results of five representative RCs (Fig. 3A), we proceeded to evaluate the recoveries of several standard RCs that had been added to mouse plasma samples. The recoveries of the RCs tested in the current study were in the range of 70.3–111.8% (Table 1). The corresponding calibration curves, which were obtained by plotting the peak area ratios of the 33 different RCs tested in the current study (tests were conducted at six different concentrations in the range of 2.5–2500 fmol) relative to IS exhibited good linearities ($r^2>0.9964$) (Table 1). The LOD values (S/N = 5) were found to be in the range of 1–20 fmol, and the LOQ values (S/N = 10) were in the range of 1–50 fmol on column. The assay precision was examined using mouse plasma samples spiked with two different concentrations of the RCs (Table 2). The RSD values were found to be <19.3% for the intra- and inter-day precision measurements, and the accuracy rates ranged from 75.4 to 119.9% (Table 2). These results effectively indicated that the current method is highly accurate and reproducible. Furthermore, the good linearity, sensitivity, recovery and precision properties of this method suggested that it could be used for the analysis of other human and animal tissue samples.

RCs are organic compounds that are widespread in biological samples. Compounds of this type can be formed from fatty acids,

Table 2
Accuracy (analytical recoveries) and precision of the assay used for the determination of the RCs in mice plasma.

Compound		Added (pmol/mL)	Measured (pmol/mL)[a]	RSD (%)	Accuracy (%)	Compound		Added (pmol/mL)	Measured (pmol/mL)[a]	RSD (%)	Accuracy (%)
Acrolein	Intra-day	–	146.5 ± 13.0	8.9	–	Nonanal	Intra-day	–	652.0 ± 7.9	1.2	–
		100	235.2 ± 20.5	8.7	88.7			500	1073.9 ± 59.5	5.5	84.4
		500	680.4 ± 36.2	5.3	106.8			1000	1518.8 ± 18.4	1.2	86.7
	Inter-day	–	153.6 ± 26.3	17.1	–		Inter-day	–	653.6 ± 27.1	4.1	–
Glyoxal	Intra-day	–	52.0 ± 1.3	2.4	–	2,4-DDE	Intra-day	–	9.4 ± 1.1	11.8	–
		50	108.3 ± 4.2	3.9	112.8			50	64.9 ± 1.2	1.8	110.1
		100	158.1 ± 4.4	2.8	106.1			100	110.1 ± 3.3	3.0	100.7
	Inter-day	–	56.3 ± 3.0	5.3	–		Inter-day	–	9.2 ± 1.1	12.3	–
Propanal	Intra-day	–	58.3 ± 3.8	6.5	–	HNE	Intra-day	–	16.8 ± 1.0	6.1	–
		50	178.2 ± 2.9	1.6	119.9			50	68.2 ± 1.5	2.3	102.7
		100	291.1 ± 1.4	0.5	116.4			100	120.8 ± 2.0	1.6	104.0
	Inter-day	–	59.7 ± 4.0	6.8	–		Inter-day	–	16.6 ± 0.4	2.4	–
Crotonaldehyde	Intra-day	–	14.8 ± 1.7	11.4	–	Decanal	Intra-day	–	493.0 ± 24.6	5.0	–
		50	68.1 ± 1.3	1.9	106.6			500	869.9 ± 36.1	4.1	75.4
		100	118.3 ± 0.6	0.5	103.5			1000	1442.4 ± 30.1	2.1	94.9
	Inter-day	–	15.4 ± 1.8	11.6	–		Inter-day	–	492.2 ± 35.2	7.2	–
Butanal	Intra-day	–	101.4 ± 10.5	10.3	–	EDE	Intra-day	–	1.7 ± 0.1	3.9	–
		100	202.1 ± 10.0	5.0	100.7			50	49.2 ± 0.6	1.2	95.0
		500	605.5 ± 78.8	13.0	100.8			100	103.0 ± 3.2	3.1	101.1
	Inter-day	–	97.0 ± 16.0	16.5	–		Inter-day	–	1.7 ± 0.1	3.9	–
Pentanal	Intra-day	–	65.0 ± 8.1	12.4	–	2-Undecenal	Intra-day	–	4.3 ± 0.5	11.5	–
		50	121.0 ± 13.5	11.2	112.0			50	57.1 ± 1.8	3.2	105.8
		100	155.9 ± 8.6	5.5	90.9			100	105.6 ± 2.5	2.4	101.4
	Inter-day	–	66.8 ± 6.6	9.9	–		Inter-day	–	1.7 ± 0.5	15.9	–
2-HxDE	Intra-day	–	<LOQ	–	–	Undecanal	Intra-day	–	106.3 ± 9.1	8.5	–
		50	53.0 ± 5.7	10.8	105.9			100	189.0 ± 7,4	3.9	82.7
		100	102.0 ± 4.3	4.2	102.0			500	622.0 ± 6.7	1.1	103.1
	Inter-day	–	<LOQ	–	–		Inter-day	–	105.6 ± 7.6	7.6	–
2-Hexenal	Intra-day	–	4.4 ± 0.4	9.0	–	Dodecanal	Intra-day	–	740.5 ± 44.6	6.0	–
		50	53.8 ± 1.6	3.0	98.7			500	1209.6 ± 21.5	1.8	93.8
		100	108.1 ± 1.6	1.5	103.7			1000	1622.8 ± 45.1	2.8	88.2
	Inter-day	–	4.6 ± 0.4	8.4	–		Inter-day	–	745.1 ± 42.6	5.7	–
Hexanal	Intra-day	–	60.0 ± 3.2	5.3	–	Tridecanal	Intra-day	–	151.0 ± 5.0	3.0	–
		50	119.9 ± 23.2	19.3	119.7			100	237.8 ± 6.2	2.6	86.8
		100	155.1 ± 13.9	9.0	95.1			500	631.4 ± 10.4	1.7	96.1
	Inter-day	–	58.7 ± 5.7	9.7	–		Inter-day	–	146.7 ± 7.0	4.7	–
2-HpDE	Intra-day	–	4.7 ± 0.8	16.9	–	Tetradecanal	Intra-day	–	174.3 ± 18.6	10.7	–
		50	59.6 ± 4.0	6.7	109.8			100	272.1 ± 20.5	7.5	97.8
		100	106.0 ± 7.1	6.7	101.3			500	708.9 ± 12.1	1.7	106.9
	Inter-day	–	5.5 ± 0.6	10.3	–		Inter-day	–	177.5 ± 8.4	4.7	–
2-Heptenal	Intra-day	–	5.1 ± 0.4	7.1	–	Pentadecanal	Intra-day	–	188.7 ± 12.8	6.8	–
		50	56.5 ± 0.7	1.2	102.9			100	280.1 ± 23.5	8.4	91.4
		100	106.6 ± 4.1	3.8	101.5			500	664.9 ± 20.7	3.1	95.3
	Inter-day	–	4.8 ± 0.2	3.5	–		Inter-day	–	186.4 ± 13.3	7.1	–
HHE	Intra-day	–	7.1 ± 0.5	6.5	–	Hexadecanal	Intra-day	–	630.8 ± 43.6	6.9	–
		50	57.9 ± 2.6	4.5	101.5			500	1110.9 ± 29.8	2.7	96.0
		100	107.9 ± 4.3	4.0	100.8			1000	1521.3 ± 42.0	2.8	89.1
	Inter-day	–	7.0 ± 0.1	1.6	–		Inter-day	–	634.5 ± 42.8	6.7	–
Heptanal	Intra-day	–	55.1 ± 4.2	7.5	–	Heptadecanal	Intra-day	–	31.2 ± 3.7	11.9	–
		50	102.2 ± 9.0	8.8	94.2			50	84.9 ± 6.7	7.9	107.3
		100	149.9 ± 6.2	4.2	94.9			100	131.2 ± 10.1	7.7	100.0
	Inter-day	–	55.7 ± 6.7	11.9	–		Inter-day	–	31.0 ± 3.3	10.6	–
2-Octenal	Intra-day	–	9.0 ± 0.7	8.1	–	Octadecanal	Intra-day	–	300.8 ± 28.1	9.3	–
		50	58.9 ± 3.2	5.4	99.9			500	729.6 ± 17.1	2.3	85.8
		100	101.3 ± 4.3	4.2	92.3			1000	1113.5 ± 26.9	2.4	81.3
	Inter-day	–	8.9 ± 1.5	16.5	–		Inter-day	–	302.5 ± 27.5	9.1	–
Octanal	Intra-day	–	134.7 ± 11.0	8.1	–	Secosterol-A	Intra-day	–	2.3 ± 0.2	7.4	–
		100	218.9 ± 6.0	2.8	84.8			50	48.4 ± 1.3	2.8	92.1
		500	624.6 ± 21.8	3.5	98.0			100	95.3 ± 6.7	7.1	93.0
	Inter-day	–	132.5 ± 13.4	10.1	–		Inter-day	–	2.3 ± 0.1	2.5	–
2,4-NDE	Intra-day	–	3.8 ± 0.2	5.8	–	Secosterol-B	Intra-day	–	5.9 ± 0.4	6.1	–
		50	52.6 ± 2.8	5.3	97.5			50	49.7 ± 2.5	4.9	87.6
		100	103.1 ± 3.2	3.1	99.2			100	99.4 ± 2.9	2.9	93.5
	Inter-day	–	3.8 ± 0.2	6.0	–		Inter-day	–	5.7 ± 0.2	3.8	–
2-Nonenal	Intra-day	–	20.2 ± 1.7	8.6	–						
		50	67.5 ± 1.4	2.1	94.6						
		100	116.7 ± 3.4	3.0	96.4						
	Inter-day	–	20.2 ± 1.4	6.9	–						

[a] $n = 3$.

amino acids, and aromatic compounds, as well as several other compound classes. The results of a growing number of studies have suggested that RCs could be involved in the development of oxidative stress related disorders, such as cancer, cardiovascular disease, neurodegenerative disease and diabetes, as well as several other diseases associated with aging. Our newly developed method would allow for the exploration of different RCs regardless of their chemical structure, and represents a particularly powerful

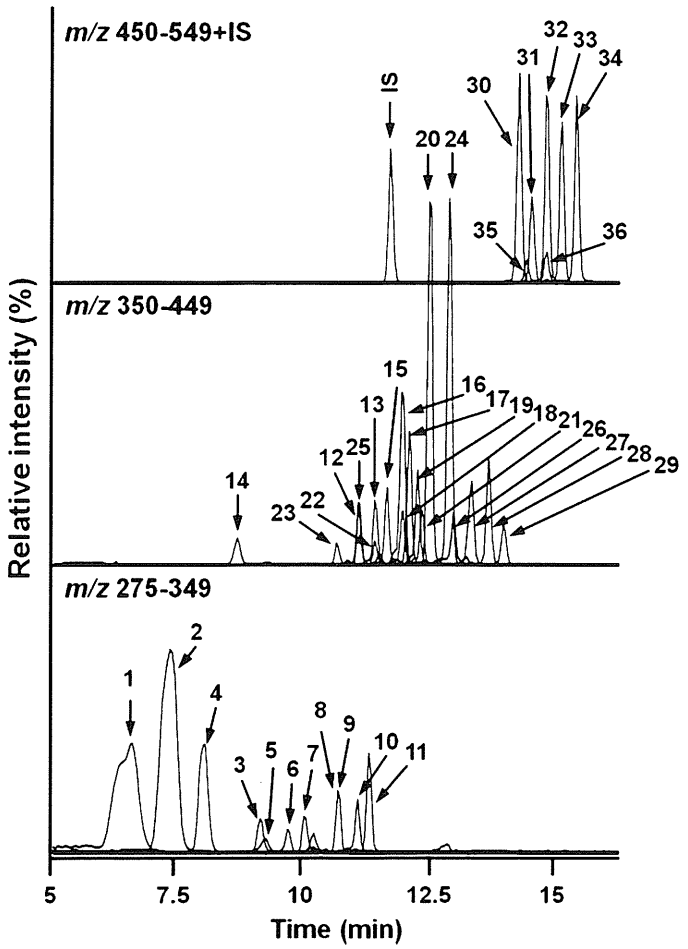

Fig. 2. LC/ESI-MS/MS (SRM) chromatogram of a standard mixture of the RC-DH derivatives (0.5 pmol each). The SRM assay detected the characteristic product ion of the 5-dimethylaminonaphthalene-1-sulfonyl moiety (*m/z* 236.1), which was derived from the positively ionized RC-DH derivatives transmitting the $[M+H]^+ \rightarrow 236.1$ transition. The peak numbers indicate the names of the RCs as follows: (1) formaldehyde (t_R:7.5 min, *m/z* 278); (2) acetaldehyde (t_R:7.5 min, *m/z* 292); (3) acrolein (t_R:9.3 min, *m/z* 304); (4) glyoxal (t_R:8.4 min, *m/z* 306); (5) propanal (t_R:9.3 min, *m/z* 306); (6) crotonaldehyde (t_R:9.8 min, *m/z* 318); (7) butanal (t_R:10.1 min, *m/z* 320); (8) pentanal (t_R:10.8 min, *m/z* 334); (9) 2,4-HxDE (t_R:10.8 min, *m/z* 344); (10) 2-hexenal (t_R:11.1 min, *m/z* 346); (11) hexanal (t_R:11.3 min, *m/z* 348); (12) 2,4-HpDE (t_R:11.2 min, *m/z* 358); (13) 2-heptenal (t_R:11.6 min, *m/z* 360); (14) HHE (t_R:8.9 min, *m/z* 362); (15) heptanal (t_R:11.8 min, *m/z* 362); (16) 2-octenal (t_R:12.0 min, *m/z* 374); (17) octanal (t_R:12.2 min, *m/z* 376); (18) 2,4-NDE (t_R:12.2 min, *m/z* 386); (19) 2-nonenal (t_R:12.4 min, *m/z* 388); (20) nonanal (t_R:12.6 min, *m/z* 390); (21) 2,4-DDE (t_R:12.5 min, *m/z* 400); (22) ONE (t_R:11.5 min, *m/z* 402); (23) HNE (t_R:10.8 min, *m/z* 404); (24) decanal (t_R:13.0 min, *m/z* 404); (25) EDE (t_R:11.3 min, *m/z* 416); (26) 2-undecenal (t_R:13.1 min, *m/z* 416); (27) undecanal (t_R:13.3 min, *m/z* 418); (28) dodecanal (t_R:13.6 min, *m/z* 432); (29) tridecanal (t_R:13.9 min, *m/z* 446); (30) tetradecanal (t_R:14.3 min, *m/z* 460); (31) pentadecanal (t_R:14.6 min, *m/z* 474); (32) hexadecanal (t_R:14.8 min, *m/z* 488); (33) heptadecanal (t_R:15.1 min, *m/z* 502); (34) octadecanal (t_R:15.4 min, *m/z* 516); (35) secosterol-A (t_R:14.4 min, *m/z* 666); (36) secosterol-B (t_R:14.8 min, *m/z* 666); (IS) *p*-BOBA (t_R:11.8 min, *m/z* 460).

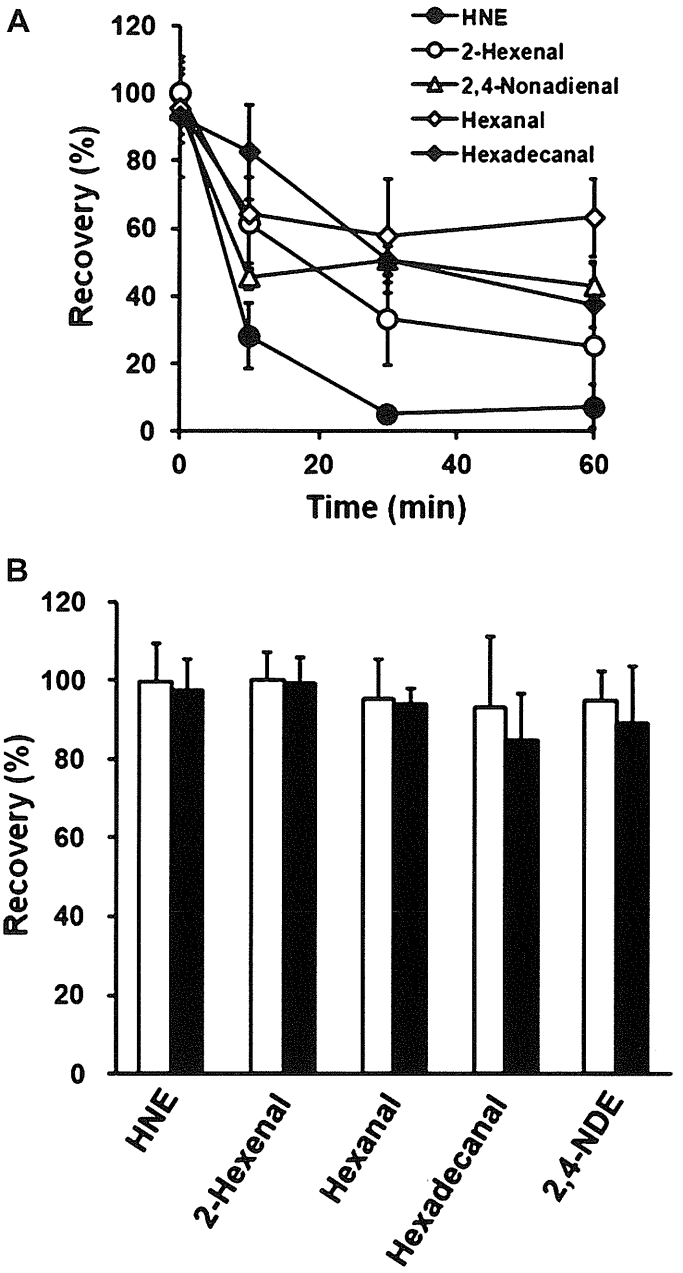

Fig. 3. Stabilities of the RCs in mice plasma. The plasma samples (100 μL) were spiked with five representative RCs, such as 4-hydroxy-2-alkenal (HNE), 2-alkenal (2-hexenal), and 2,4-alkadienal (2,4-NDE), as well as a short chain alkanal (hexanal) (5 pmol each) and a long chain alkanal (hexadecanal) (100 pmol). The spiked samples were stored on ice for 0–60 min (A) or stored at −80 °C for 4 weeks (B). The open and closed bars represent the recoveries of the RCs, which were determined immediately before and after being stored at −80 °C for 4 weeks.

analytical platform for studying the roles of RCs in the development and progression of oxidative stress related-disorders.

3.3. *Comprehensive analyses of the lipophilic RCs present in mouse plasma samples*

Our newly developed method was used to analyze the RC profiles of plasma samples obtained from C57BL/6J mice (10 weeks of age). Fig. 4 shows SRM chromatograms typical of those obtained for the free RCs detected in the mouse plasma samples. Fig. 5A shows the corresponding RCs maps, where all of the free RCs detected in the mouse plasma samples were plotted as circles as a function of their retention times (horizontal axis) and *m/z* values (vertical axis). The areas of the circles represent the intensities of peaks for the detected RCs relative to that of IS.

Four hundred and five peaks were detected in the plasma samples obtained from the normal C57BL/6J mice (based on an average of five determinations) following the elimination of the redundant peaks from the spectra, including the spike noise and artifactual DH derivatives (e.g., some of the solvents used in the current study were found to be contaminated with RCs). The RCs detected in the mouse plasma samples using this method were considered to be free RCs or those liberated from unstable Schiff base adducts.

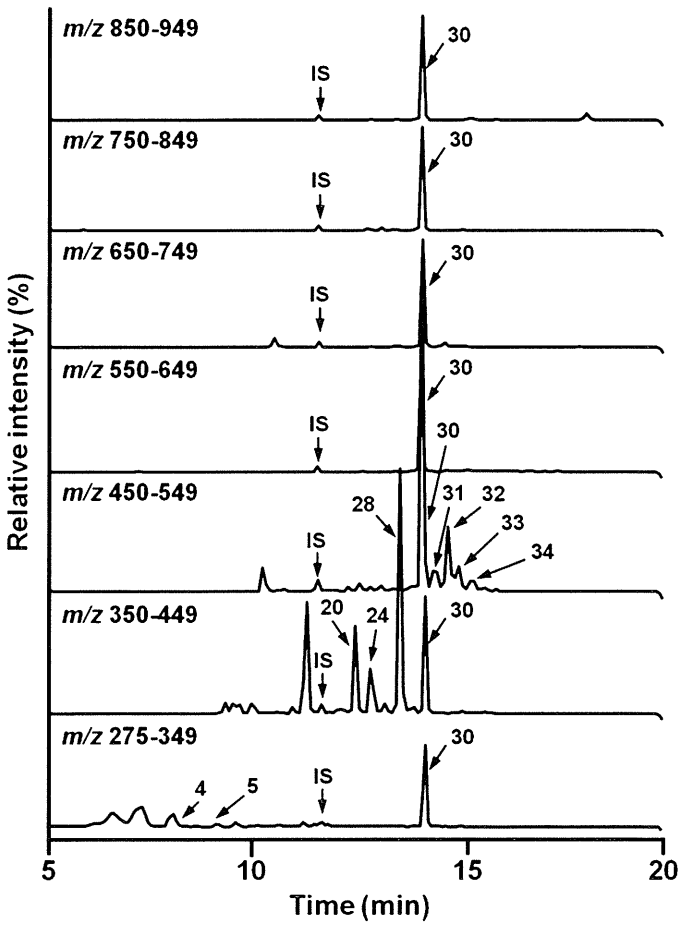

Fig. 4. Representative SRM chromatograms of the RC-DH derivatives, which were detected in the plasma samples obtained from normal C57BL/6J mice.

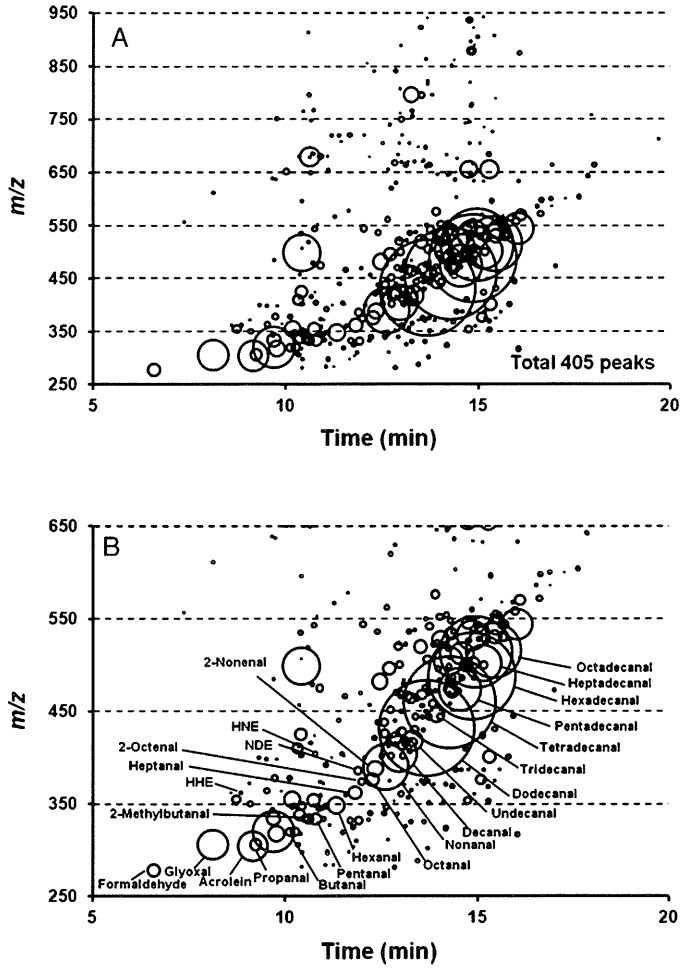

Fig. 5. RC maps of the plasma samples obtained from normal C57BL/6J mice (A). An enlarged view showing the names of some of the RCs identified through a comparison of their data with those of the authentic standards in Fig. 5A (B). In the RC map, the different RCs detected are shown as circles as a function of their LC retention times (horizontal axis) and *m/z* values (vertical axis). The area of each circle represents the relative intensity of the RC to that of IS.

Fig. 5B is an enlarged view of Fig. 5A, showing *m/z* values in the range of 250–650, together with the names of some of the RCs identified through a comparison of their data with those of the authentic RCs. A series of low molecular weight aldehydes, including formaldehyde (t_R: 6.8 min, *m/z* 278), acetaldehyde (t_R: 7.5 min, *m/z* 292), acrolein (t_R: 9.3 min, *m/z* 304), glyoxal (t_R: 8.4 min, *m/z* 306) and propanal (t_R: 9.3 min, *m/z* 306) are shown in the bottom left corner in Fig. 5B. Several large circles also appeared side by side on the diagonal in the center of the figure. As the retention times increased, the molecular weights of these peaks increased in *m/z* increments of 14. Based on a comparison of these peaks with those of the authentic RCs, it was established that they corresponded to several fatty aldehydes, including hexanal ($C_6H_{12}O$, t_R: 11.3 min, *m/z* 348), nonanal ($C_9H_{18}O$, t_R: 12.6 min, *m/z* 390) and hexadecanal ($C_{16}H_{32}O$, t_R: 14.8 min, *m/z* 488). Dodecanal ($C_{12}H_{24}O$) was determined to be the most abundant peak in the chromatogram with a retention time of 13.6 min and an *m/z* value of 432. Low concentrations of HHE (t_R: 8.9 min, *m/z* 362), NDE (t_R: 12.1 min, *m/z* 386), DDE (t_R: 12.5 min, *m/z* 400), ONE (t_R: 11.5 min, *m/z* 402), HNE (t_R: 10.8 min, *m/z* 404) and EDE (t_R: 11.3 min, *m/z* 416) were also detected. These RCs are known oxidation products, which are derived from PUFAs, such as linoleic acid (LA), arachidonic acid (AA) and docosahexaenoic acid (DHA). Acrolein can be derived from the oxidation of either DHA or AA, whereas hexanal and HNE can be derived from the oxidation of AA and LA. HHE is the major product of the oxidation of DHA and other ω-3 PUFAs [21–28].

A variety of fatty aldehydes between C1 (formaldehyde) and C18 (octadecanal) were detected in the plasma samples obtained from normal C57BL/6J mice (Fig. 5), with some of these fatty aldehydes being detected in large concentrations. Fatty aldehydes have been reported to undergo further biotransformations to afford fatty acids and alcohols [4,26,28–31]. Hexadecanal has been reported to form as one of the major products of the sphigosine-1-phosphate lyase-mediated degradation of dihydrosphingosine-1-phosphate (DHS1P) [32].

The peak with a retention time of 10.5 min and an *m/z* value of 334 was attributed to 2-methylbutanal, which has been reported to be formed by the oxidation of the aliphatic amino acid L-isoleucine with a myeloperoxidase-H_2O_2-chloride system [33].

Our newly developed method can be used to detect a large number of different free lipophilic RCs (regardless of their structure) including alkanals (e.g., hexanal and hexadecanal), 2-alkenals (e.g., 2-nonenal) and 4-hydroxy-2-alkenals (e.g., HNE and ONE), as well as structurally unknown RCs.

During the course of the current study, Siegel et al. [34] reported a similar method for the quantification and identification of various RCs in biological samples. Siegel's method involved the derivatization of RCs with *p*-toluensulfonylhydrazine and the subsequent detection of the derivatives by ultrahigh-performance liquid chromatography with ESI-MS. We believe that our newly developed method is comparable with that of Siegel et al. [34] in term of its specificity, sensitivity and repeatability properties for the analysis of a wide variety of RCs.

4. Conclusion

We have developed a novel analytical method for profiling the wide variety of different lipophilic RCs present in biological samples using LC/ESI-MS/MS with SRM. The method was found to be sensitive, reproducible, accurate and specific for RCs, and the analytical results obtained in the current were expressed as RC maps, which allowed for the types and levels of the different lipophilic RCs to be readily visualized. The results revealed that a large number of unidentified RCs were present in the mice plasma samples, and further studies are therefore needed to identify the structures of these compounds. This newly developed approach could be very useful for establishing the RC profiles of biological and environmental samples, as well as for studying the roles of lipid peroxidation in oxidative stress related-disorders and discovering new biomarkers for the early diagnosis of these diseases.

Acknowledgments

This work was supported in part by grants from the Japan Society for the Promotion of Science (JSPS) KAKENHI (grant nos. 24700838, 24680075 and 24300257 for ST, NM, and HO, respectively). This study was also supported by grants from the National Cancer Center Research and Development Fund 23-A-4 and 26-A-8) and Grants-in-Aids [Risk of Chemical Substance 2524301 (H25-Kagaku-ippan-004)] from the Ministry of Health, Labor and Welfare, Japan.

References

[1] M. Masoodi, A.A. Mir, N.A. Petasis, C.N. Serhan, A. Nicolaou, Simultaneous lipidomic analysis of three families of bioactive lipid mediators leukotrienes, resolvins, protectins and related hydroxy-fatty acids by liquid chromatography/electrospray ionisation tandem mass spectrometry, Rapid Commun. Mass Spectrom. 22 (2008) 75–83.
[2] E. Niki, Lipid peroxidation: physiological levels and dual biological effects, Free Radic. Biol. Med. 47 (2009) 469–484.
[3] F. Gueraud, M. Atalay, N. Bresgen, A. Cipak, P.E. Eckl, L. Huc, I. Jouanin, W. Siems, K. Uchida, Chemistry and biochemistry of lipid peroxidation products, Free Radic. Res. 44 (2010) 1098–1124.
[4] P.J. O'Brien, A.G. Siraki, N. Shangari, Aldehyde sources, metabolism, molecular toxicity mechanisms, and possible effects on human health, Crit. Rev. Toxicol. 35 (2005) 609–662.
[5] P.A. Grimsrud, H. Xie, T.J. Griffin, D.A. Bernlohr, Oxidative stress and covalent modification of protein with bioactive aldehydes, J. Biol. Chem. 283 (2008) 21837–21841.
[6] S. Bacot, N. Bernoud-Hubac, N. Baddas, B. Chantegrel, C. Deshayes, A. Doutheau, M. Lagarde, M. Guichardant, Covalent binding of hydroxy-alkenals 4-HDDE, 4-HHE, and 4-HNE to ethanolamine phospholipid subclasses, J. Lipid Res. 44 (2003) 917–926.
[7] S. Bacot, N. Bernoud-Hubac, B. Chantegrel, C. Deshayes, A. Doutheau, G. Ponsin, M. Lagarde, M. Guichardant, Evidence for in situ ethanolamine phospholipid adducts with hydroxyl-alkenals, J. Lipid Res. 48 (2007) 816–825.
[8] R.G. Salomon, X. Gu, Critical insights into cardiovascular disease from basic research on the oxidation of phospholipids: the γ-hydroxyalkenal phospholipid hypothesis, Chem. Res. Toxicol. 24 (2011) 1791–1802.
[9] W. Völkel, R. Alvarez-Sánchez, J. Weick, A. Mally, W. Dekant, A. Pähler, Glutathione conjugates of 4-hydroxy-2(E)-nonenal as biomarkers of hepatic oxidative stress-induced lipid peroxidation in rats, Free Radic. Biol. Med. 38 (2005) 1526–1536.
[10] W. Jian, S.H. Lee, C. Mesaros, T. Oe, M.V. Elipe, I.A. Blair, A novel 4-oxo-2(E)-nonenal-derived endogeneous thiadiazabicylo glutathione adduct formed during cellular oxidative stress, Chem. Res. Toxicol. 20 (2007) 1008–1018.
[11] K. Uchida, Role of reactive aldehyde in cardiovascular diseases, Free Radic. Biol. Med. 28 (2000) 1685–1696.
[12] U. Nair, H. Bartsch, J. Nair, Lipid peroxidation-induced DNA damage in cancer-prone inflammatory diseases: a review of published adduct types and levels in humans, Free Radic. Biol. Med. 43 (2007) 1109–1120.
[13] X.P. Luo, M. Yazdanpanah, N. Bhooi, D.C. Lehotay, Determination of aldehydes and other lipid peroxidation products in biological samples by gas chromatography–mass spectrometry, Anal. Biochem. 228 (1995) 294–298.
[14] G.A. Cordis, D.K. Das, W. Riedel, High-performance liquid chromatographic peak identification of 2,4-dinitrophenylhydrazine derivatives of lipid peroxidation aldehydes by photodiode array detection, J. Chromatogr. A 798 (1998) 117–123.
[15] C. Zwiener, T. Glauner, F.H. Frimmel, Method optimization for the determination of carbonyl compounds in disinfected water by DNPH derivatization and LC/ESI-MS-MS, Anal. Bioanal. Chem. 372 (2002) 615–621.
[16] S. Tomono, N. Miyoshi, K. Sato, Y. Ohba, H. Ohshima, Formation of cholesterol ozonolysis products through an ozone-free mechanism mediated by the myeloperoxidase-H_2O_2-chloride system, Biochem. Biophys. Res. Commun. 383 (2009) 222–227.
[17] S. Tomono, N. Miyoshi, H. Shiokawa, T. Iwabuchi, Y. Aratani, T. Higashi, H. Nukaya, H. Ohshima, Formation of cholesterol ozonolysis products in vitro and in vivo through a myeloperoxidase-dependent pathway, J. Lipid Res. 52 (2011) 87–97.
[18] N. Miyoshi, N. Iwasaki, S. Tomono, T. Higashi, H. Ohshima, Occurrence of cytotoxic 9-oxononanoyl secosterol aldehydes in human low-density lipoprotein, Free Radic. Biol. Med. 60 (2013) 73–79.
[19] D.K. Dalvie, J.P. O'Donnell, Characterization of polar urinary metabolites by ion-spray tandem mass spectrometry following dansylation, Rapid Commun. Mass Spectrom. 12 (1998) 419–422.
[20] P. Wentworth Jr., J. Nieva, C. Takeuchi, R. Galve, A.D. Wentworth, R.B. Dilley, G.A. DeLaria, A. Saven, B.M. Babior, K.D. Janda, A. Eschenmoser, R.A. Lerner, Evidence for ozone formation in human atherosclerotic arteries, Science 302 (2003) 1053–1056.
[21] T. Kaneko, S. Honda, S. Nakano, M. Matsuo, Lethal effects of a linoleic acid hydroperoxide and its autooxidation products, unsaturated aliphatic aldehydes, on human diploid fibroblasts, Chem. Biol. Interact. 63 (1987) 127–137.
[22] T. Kaneko, K. Kaji, M. Matsuo, Cytotoxicities of a linoleic acid hydroperoxide and its related aliphatic aldehydes toward cultured human umbilical vein endothelial cells, Chem. Biol. Interact. 67 (1988) 295–304.
[23] J.K. Beckman, M.J. Howard, H.L. Greene, Identification of hydroxyalkenals formed from omega-3 fatty acids, Biochem. Biophys. Res. Commun. 169 (1990) 75–80.
[24] F.J. Van Kuijk, L.L. Holte, E.A. Dratz, 4-Hydroxyhexenal: a lipid peroxidation product derived from oxidized docosahexaenoic acid, Biochim. Biophys. Acta 1043 (1990) 116–118.
[25] S.H. Lee, T. Oe, I.A. Blair, Vitamin C-induced decomposition of lipid hydroperoxides to endogenous genotoxins, Science 292 (2001) 2083–2086.
[26] P. Spiteller, W. Kern, J. Reiner, G. Spiteller, Aldehydic lipid peroxidation products derived from linoleic acid, Biochem. Biophys. Acta 1531 (2001) 188–208.
[27] K. Warner, W.E. Neff, W.C. Byrdwell, H.W. Gardner, Effect of oleic and linoleic acid on the production of deep-fried odor in heated triolein and trilinolein, J. Agric. Food Chem. 49 (2001) 899–905.
[28] Y. Kawai, S. Takeda, J. Terao, Lipidomic analysis for lipid peroxidation-derived aldehydes using gas chromatography-mass spectrometry, Chem. Res. Toxicol. 20 (2007) 99–107.
[29] H. Esterbauer, G. Jurgens, O. Quehenberger, E. Koller, Autoxidation of human low density lipoprotein: loss of polyunsaturated fatty acid and vitamin E and generation of aldehydes, J. Lipid Res. (1987) 495–509.
[30] S. Stadelmann-Ingrand, S. Favreliere, B. Fauconneau, G. Mauco, C. Tallineau, Plasmalogen degradation by oxidative stress: production and disappearance of specific fatty aldehydes and fatty alpha-hydroxyaldehydes, Free Radic Biol. Med. 31 (2001) 1263–1271.
[31] K. Watschinger, E.R. Werner, Alkylglycerol monooxygenase, IUBMB Life 65 (2013) 366–372.
[32] E.V. Berdyshev, J. Goya, I. Gorshkova, G.D. Prestwich, H.S. Byun, R. Bittman, V. Natarajan, Characterization of sphingosine-1-phosphate lyase activity by electrospray ionization-liquid chromatography/tandem mass spectrometry quantitation of (2E)-hexadecenal, Anal. Biochem. 408 (2011) 12–18.
[33] S.L. Hazen, F.F. Hsu, A. d'Avignon, J.W. Heinecke, Human neutrophils employ myeloperoxidase to convert alpha-amino acids to a battery of reactive aldehydes: a pathway for aldehyde generation at sites of inflammation, Biochemistry 37 (1998) 6864–6873.
[34] D. Siegel, A.C. Meinema, H. Permentier, G. Hopfgartner, R. Bischoff, Integrated quantification and identification of aldehydes and ketones in biological samples, Anal. Chem. 86 (2014) 5089–5100.

Advanced Drug Delivery Reviews 99 (2016) 206–211

Contents lists available at ScienceDirect

Advanced Drug Delivery Reviews

journal homepage: www.elsevier.com/locate/addr

Heterogeneity of tumor cells in the bone microenvironment: Mechanisms and therapeutic targets for bone metastasis of prostate or breast cancer☆

Mitsuru Futakuchi *, Katsumi Fukamachi, Masumi Suzui

Department of Molecular Toxicology, Graduate School of Medical Sciences, Nagoya City University, Nagoya 467-8601, Japan

ARTICLE INFO

Article history:
Received 31 May 2015
Received in revised form 19 November 2015
Accepted 25 November 2015
Available online 4 December 2015

Keywords:
Bone microenvironment
Bone metastasis
Tumor stromal interaction
Metastatic cascade prostate cancer
Breast cancer

ABSTRACT

Bone is the most common target organ of metastasis of prostate and breast cancers. This produces considerable morbidity due to skeletal-related events, SREs, including bone pain, hypercalcemia, pathologic fracture, and compression of the spinal cord. The mechanism of bone metastasis is complex and involves cooperative reciprocal interaction among tumor cells, osteoblasts, osteoclasts, and the mineralized bone matrix. The interaction between the metastatic tumor and bone stromal cells has been commonly referred to as the "vicious cycle". Tumor cells stimulate osteoblasts, which in turn stimulate osteoclasts through the secretion of cytokines such as the TNF family member receptor activator of nuclear κB ligand (RANKL). Activated osteoclasts degrade the bone matrix by producing strong acid and proteinases. Bone degradation by osteoclasts releases TGFβ and other growth factors stored in the bone matrix, that further stimulate tumor cells. Bone modifying agents, targeting osteoclast activity, such as bisphosphonate and RANKL antibodies are considered as the standard of care for reducing SREs of patients with bone metastatic diseases. These agents decrease osteoclast activity and delay worsening of skeletal pain and aggravation of bone metastatic diseases. While the management of SREs by these agents may improve patients' lives, this treatment does not address the specific issues of the patients with bone metastasis such as tumor dormancy, drug resistance, or improvement of survival. Here, we review the mechanisms of bone metastasis formation, tumor heterogeneity in the bone microenvironment, and conventional therapy for bone metastatic diseases and discuss the potential development of new therapies targeting tumor heterogeneity in the bone microenvironment.

Contents

1. Introduction

Tumor metastasis is multiple processes, that involves involve invasion, embolization, survival in the circulation, arrest in a distant capillary bed, extravasation, and re-growth in the microenvironment of the secondary organ [1] (Fig. 1). Metastatic tumor cells are required to

☆ This review is part of the *Advanced Drug Delivery Reviews* theme issue on "Insights into heterogeneity in tumor microenvironment for drug development".

* Corresponding author. Tel.: +81 52 853 8992; fax: +81 52 853 8996.
E-mail address: futakuch@med.nagoya-cu.ac.jp (M. Futakuchi).

http://dx.doi.org/10.1016/j.addr.2015.11.017
0169-409X/

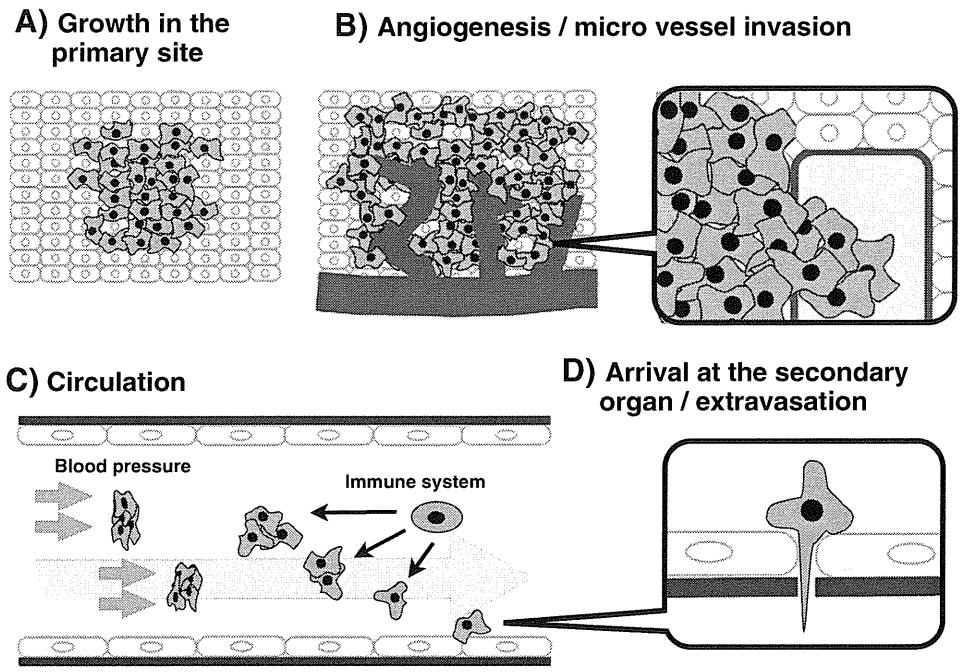

Fig. 1. Metastatic Cascade. A. Tumor growth at the primary site. Tumor growth at the primary site is progressive with nutrients for the expanding tumor mass initially supplied by simple diffusion. B. Angiogenesis/microvessel invasion. The synthesis and secretion of angiogenic factors establish a capillary network from the surrounding tumor tissue. C. Circulation. After detachment from the primary site, tumor cells need to survive the mechanical stress of blood pressure and attack from the immune system in the circulation. D: Arrival at the secondary organ/extravasation. After the tumor cells have survived the circulation, they are trapped in the capillary beds of distant organs. Thin-walled venules, such as lymphatic channels, offer very little resistance to penetration by tumor cells and provide the most common route for tumor-cell entry into the tissue.

complete all of these processes to form metastases. Metastatic tumor cells are often compared to a decathlon athlete who is skilled in all ten track and field events [2]. Because tumor cells are exposed to the host response in each process [3], the vast majority of potentially metastatic cells from the primary tumor, which are often detected in the serum of advanced cancer patients [4], are eliminated before they are able to successfully form a metastasis. Therefore, tumor metastasis is a selective process, and through this process results in phenotypic diversification of the metastatic tumor cells arise from the genetically and phenotypically unstable primary tumor [5]. Although only a few cells from a primary tumor are able to give rise to a metastasis [6,7], the tumor cells with metastasis phenotype gained through the selective cascade of metastasis can provide new insight into the biological heterogeneity of metastatic tumor cells.

2. Mechanism for bone metastasis

Bone is the most common organ of metastasis of two of the most common cancers, prostate and breast cancers. Bone metastasis is particularly clinical important because of the consequent morbidity and complex demands on health care resources. The clinical symptoms of bone metastases can be extensive, often accounting for the poor prognosis of patients with bone metastasis that is associated with advanced prostate or breast cancer.

There are different patterns in the metastatic bone lesions, ranging from mostly destructive or osteolytic to mostly bone forming or osteoblastic, based on the radiographic or histological observation of the bone metastatic lesion. The homeostatic balance between resorption and formation in the bone is clearly dysregulated in bone metastases. In breast cancer bone metastases, although the dominant bone lesion is destructive and osteolytic, local bone forming and osteoblastic lesions are also observed [8]. Similarly, in the case of prostate cancer, although bone lesions are diagnosed as bone forming and osteoblastic, it is clear that destructive, osteolytic lesions play important roles in bone metastasis formation of prostate cancer. Most patients with bone metastasis regardless of cancer type would have symptoms of both osteolytic and osteoblastic change [9].

The mechanism of bone metastasis is complex and involves cooperative reciprocal interactions among tumor cells, osteoblasts, osteoclasts, and the mineralized bone matrix [10]. The excess of soluble and cellular components, signaling network, and coordinated gene expression has been shown to contribute the interplay among bone degradation, bone formation, and tumor growth. The mechanism of these interplays is gradually being unraveled. The interaction between the metastatic tumor and bone stromal cells has been commonly referred as the "vicious cycle" [8]. Tumor cells that reach in the bone microenvironment secrete factors such as parathyroid hormone related peptide (PTHrP), that stimulate osteoblasts. Activated osteoblasts increase the expression of the TNF family member receptor activator of nuclear κB ligand (RANKL) (Fig. 2). RANKL, by binding to its receptor RANK, has been shown to be essential in mediating osteoclast activation [11], and activated osteoclasts degrade the bone matrix by producing strong acid and proteinases such as the cathepsins and matrix metalloproteinases (MMPs) [12]. Bone degradation by osteoclasts releases TGFβ and other growth factors stored in the bone matrix into the bone microenvironment. These growth factors in turn stimulate tumor growth and lead to increased levels of tumor derived PTHrP (Fig. 2). This vicious cycle accelerates tumor stromal interaction in the bone microenvironment, providing a particularly fertile soil to promote aggressive behavior of the malignant tumor cells that arrived at the bone microenvironment.

Once tumor cells start re-growing in the bone microenvironment, which is manifested as bone metastatic lesions by clinical examination, most of the lesions begin to exert resistant to the conventional chemotherapy [13]. To develop new therapeutics that are effective for bone metastatic lesions, appropriate targets need to be identified and tested that would interfere with metastatic tumor cells establishing a new microenvironment. Currently, such studies are circumscribed by limited availability of appropriate animal models that precisely dissect the tumor–stromal interaction, contributing to metastatic establishment and progression.

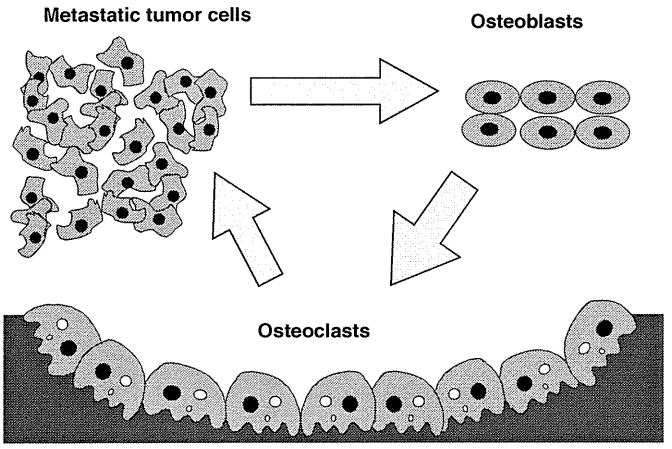

Fig. 2. Vicious cycle hypothesis. Mechanism of bone metastasis. The mechanism of bone metastasis formation has been commonly referred to as the "vicious cycle", whereby tumor cells in the bone secrete factors such as parathyroid hormone related peptide (PTHrP) that stimulate osteoblast expression of the TNF family member receptor activator of nuclear κB ligand (RANKL). Binding of RANKL to its receptor RANK has been shown to be essential in mediating osteoclast activation. The osteoclasts degrade the bone matrix using a powerful array of proteinases, and degradation of the bone matrix leads to the release of TGFβ and other growth factors that in turn stimulate tumor growth and lead to increased levels of tumor derived PTHrP. During this vicious cycle, the bone microenvironment provides a particularly fertile ground for the growth and aggressive behavior of the malignant cells that reach it.

3. Animal models for tumor–stromal interaction in the bone micro-environment

Appropriate animal models will allow us to identify therapeutic targets for bone metastases and to evaluate the effectiveness of new candidate drugs. Because *in vitro* experimental models do not effectively recapitulate tumor stromal interactions in the bone microenvironment, *in vivo* animal models are essential to elucidate the mechanisms of bone metastases formation. Presently, the lack of appropriate animal models that fully reflect the biology of bone metastasis is a major obstacle to identify the molecular mechanisms of bone metastasis and to develop therapies [14–19]. Ideally, an *in vivo* model of bone metastases should reflect the natural course of the disease and accurately simulate the disease progression commonly observed in advanced cancer patients.

The microenvironment provides appropriate conditions for the survival and proliferation of the tumor cells [20,21]. The abundance of cytokines and growth factors produced through tumor stromal interactions in the bone microenvironment are thought to facilitate the malignant behavior of tumor cells in an autocrine and/or paracrine fashion [22–24]. The production of bone metastases in established models are achieved by direct injection of tumor cells into left ventricular/intra-arterial injection [25–27].

We have developed a rat bone invasion model to observe the growth of prostate cancer cells with osteoblastic/osteolytic lesions in the bone microenvironment (Fig. 3A) [28] and a mouse bone invasion model to observe growth of breast cancer cells with osteolytic lesions [29,30]. The local areas where tumor cells interact with bone are defined as the tumor bone interface (TB-interface, Fig. 3B, rectangle), and the area with tumor cells growing away from bone as the tumor alone area (TA-area, Fig. 3B, ellipse). In histological observations of the TB-interface, we observed tumor cells growing with both osteolytic lesions mediated by osteoclasts and osteoblastic lesions mediated by osteoblasts in the bone microenvironment (Fig. 3C). The histological features of these lesions mimic those of bone metastatic lesions in human prostate and breast cancers. Comparing the TB-interface with the TA-area in our animal models allowed us to explore the molecular mechanism underlying the interactions between metastatic tumor cells and host stromal cells in the bone microenvironment in a syngeneic setting.

Although our models do not recapitulate the entire metastatic process that primary tumor cells in prostate or breast move to the typical location in the bone, our model does represent how metastatic tumor cells interact with the bone stromal cells in the bone microenvironment. A few animal models with limited use of tumor variant may encompass the entire spectrum of the metastatic processes which involves invasion, transport, arrest, adherence, extravasation, growth in different microenvironments. Among them, steps of invasion and transport do

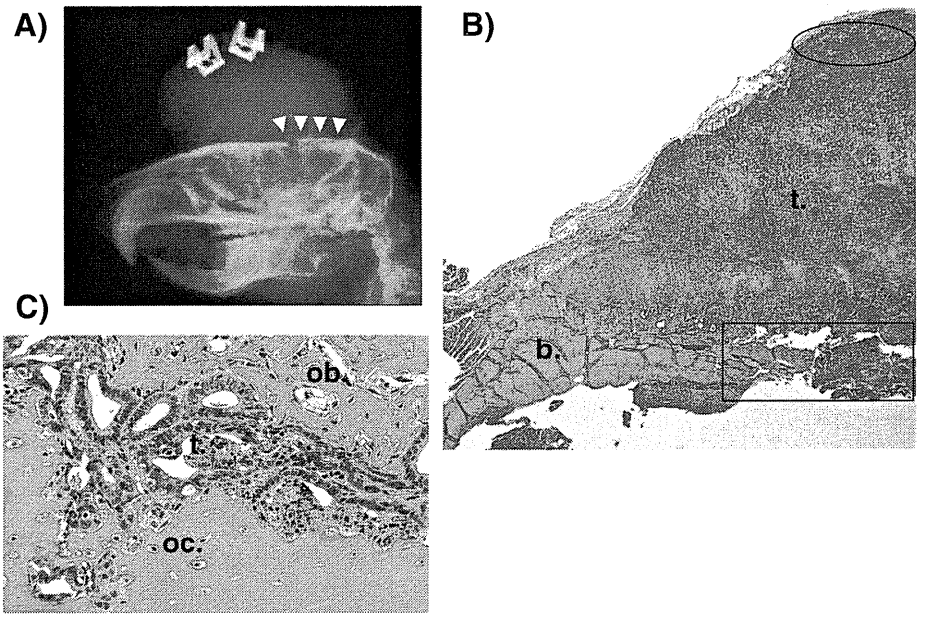

Fig. 3. Histological observations at the TB-interface. We have developed a rat bone invasion model of prostate cancer that produces osteoblastic/steolytic lesions in prostate cancer. A. X-ray analysis of the tumor 4 weeks after transplantation. Areas of osteolysis could be discerned by X-ray (indicated by white arrowheads). B. Coronal sections of the cranial bone stained with H&E at week 4. We defined the local lesions where tumor cells interacted with bone as the tumor bone interface (TB-interface, rectangle) and tumor cells away from the bone as the tumor alone area (TA-area, ellipse). b: cranial bone, t: prostate cancer tissue. C. Higher magnification of the H&E stained section at the TB-interface. Histologically, the TB-interface included tumor cells growing in the bone microenvironment (t.), osteolytic changes mediated by osteoclasts (oc.), and osteoblastic change produced by osteoblasts (ob.).

not always explain the organ specific metastasis, which is one of the important clinical features of bone metastasis. Recently, the host microenvironment has been demonstrated to be a niche for survival and growth of tumor cells [20,21]. Our "bone invasion model" has the limitation which does not recapitulate the entire process of bone metastasis, but focuses on the steps of survival and growth of the tumor in the bone microenvironment regardless of tumor type. Using our model, we identified a unique pattern of gene expression that was up-regulated at the TB interface, including genes such as RANKL, which are known to be involved in bone metastasis [31,32]. Therefore, this model provides an exciting opportunity to elucidate the molecular mechanisms underlying tumor stromal interaction in the bone microenvironment.

4. Role of RANKL in the bone microenvironment

We found that RANKL was up-regulated at the tumor bone interface in both prostate [29] and mammary models [29]. RANKL–RANK signaling is important in establishing bone metastasis because it is involved in activating the differentiation of preosteoclasts into activated osteoclasts, leading to bone resorption. This signal plays a central role in the vicious cycle [8], is up-regulated to establish osteolytic lesions.

Both RANKL and RANK proteins are bound to cell membrane. Consequently, in order to transduce RANKL–RANK signaling, physical cell-to-cell contact is required between RANKL expressing osteoblasts and RANK expressing osteoclast precursors. Since RANKL has been shown to be modulated by proteases [28,33,34], and we investigated the proteases, up-regulated at the TB-interface to determine whether they could modulate RANKL signaling to favor tumor progression. Using our prostate cancer model, we found that MMP-7 cleaved the extracellular domain of RANKL, generating an active soluble form of RANKL (sRANKL) that could activate osteoclasts and promote osteolysis using our prostate cancer model [28]. In addition, at the TB-interface of our mouse mammary tumor, we found cathepsin G, cathepsin K, matrix metalloproteinase (MMP)-9, and MMP-13 were up regulated [35], and we demonstrated that cathepsin G cleaved RANKL releasing sRANKL from the cell surface [35]. These results show that sRANKL generated by proteases in the bone microenvironment increases the number of activated osteoclasts, enhancing osteolysis. This suggests that sRANKL plays a critical role in widespread osteoclast activation in osteolytic lesions associated with bone metastatic tumors. Our data also demonstrate that proteases up-regulated in the bone microenvironment play an important role in inducing osteolytic lesions associated with the growth of metastatic tumors in the bone microenvironment by generating RANKL and contributing vicious cycle.

Interestingly, proliferation of lobulo-alveolar cells in the mammary grand during pregnancy is regulated by RANKL–RANK signaling [36] through activation of IκB kinase α (IKKα) [37]. This protein kinase also been demonstrated to be involved in proliferation of mammary cancer progenitors [38] and prostate [39] and breast cancer cells [40]. In a preliminary study, we demonstrated that RANKL inhibition led to decreased cell proliferation, which was associated with the suppression of phosphorylated IKK alpha (unpublished data). Taken together, RANKL–RANK signaling may regulate tumor cell proliferation as well as osteoclast induction in the bone microenvironment. These results suggest that sRANKL are potentially novel therapeutic target of bone metastasis of prostate and breast cancer.

5. Bone modifying agents targeting osteoclasts activity

Bone metastases associated with advanced stage prostate or breast cancer develops skeletal complications including bone pain, hypercalcemia, pathologic fracture, compression of the spinal cord, and spinal instability (also known as skeletal-related events, SREs) [41–43]. Progressive bone pain, in particular, can be severe and bothersome, as the effectiveness of analgesics, even opioid therapy is frequently declines [44–48]. The management of bone metastases can be accomplished by the combination of chemotherapy, radiation therapy and bone modifying agents such as bisphosphonate or RANKL antibody to prevent SREs [49].

Bone-modifying agents, denosumab, pamidronate, and zoledronic acid, are recommended for treatment of metastatic bone diseases [50]. Among them, zoledronic acid is approved for treatment of bone metastasis associated with castration resistant prostate cancer and denosumab has been shown to significantly increase metastasis-free survival of prostate cancer patients [51,52]. Clinical trials revealed that all these bone-modifying agents reduced the time to SRE, and SREs of breast cancer patients with bone metastasis [50]. Therefore, these agents are considered as the standard of care for reducing SREs of the patients with bone metastatic diseases [53–56]. However, the clinical trials also revealed that these bone modifying agents did not significantly prolonged the survival of the overall study population.

This has brought about a paradigm shift in the treatment of the patients, who need to preserve the quality of life (QOL) for an extended period of time because patients with metastatic disease are living longer due to improvements in cancer therapies for solid tumors. Thus, strategies in the management of metastatic bone diseases have been shifted to delay worsening of skeletal pain and aggravation of metastatic bone diseases. In fact, early palliative treatment enhanced the QOL in patients with metastatic lung cancer, which resulted in the reduction of the aggressive end-of-life care [57–59]. However, while this shift in management strategies and early intervention may improves patients' lives, these treatment do not address the specific issues of the patients with bone metastasis such as tumor dormancy, drug resistance, or improvement of survival.

6. CSC in the bone microenvironment

With the recent advent of cancer stem cell (CSC) theory, CSC activities has been identified in numerous solid tumors [60–67], including prostate [68], breast [69], and pancreas [70–72]. As discussed earlier, the process of metastasis is so inefficient that only a small subset of tumor cells that leave the primary site can successfully navigate the process of metastasis to re-initiate tumor growth to form macrometastases at distant sites.

The bone marrow regulates hematopoietic function. Hematopoietic stem cells (HSCs) are believed to localize to specific microenvironments in the bone marrow where regulation by osteoblasts, mesenchymal stem cells, adipocyctes, and CXCL12-abundant reticular (CAR) cells occurs [73–75]. In the marrow, quiescent HSCs have been demonstrated to preserve their capacity for self-renewal capable of dividing and differentiating to populate their corresponding lineages [76–78]. It is possible that such a niche would be good "soil" for CSC to grow in the bone microenvironment [79]. HSC regulating cells such as osteoblasts, bone marrow stromal cells and CAR cells may play a decisive role in maintaining CSCs in the bone microenvironment. In addition, CSCs may change the microenvironment into a more appropriate niche.

CSC is an attractive hypothesis for tumor development and progression, and coupled with the inherent tumor heterogeneity, CSCs could be involved in formation of metastases [80–84]. It is possible that CSCs in the bone microenvironment may explain the latency of bone metastasis formation, the very long period of time, a disseminated tumor cell in the bone microenvironment to grow into a gross metastasis [85]. Notably, the phenotype of a CSC may depend on the primary site and vary substantially across different microenvironments. Only CSCs specific to the bone microenvironment would contribute to bone metastasis formation. However, despite the convergence on the concept and intensive studies on CSCs, a single universal entity of CSCs was not clearly established, and the definition and identification of these cells remains elusive in most tumor types.

7. Summary and future directions

Despite significant improvements in local and systemic adjuvant therapies, bone metastases of prostate and breast cancer are still resistant to these therapies, which results in poor prognosis. Devastating skeletal complication develop in patients with bone metastatic diseases, which is the result of tumor stromal interaction in the bone microenvironment. Therapeutic agents targeting these interactions are required for management of these complications.

Strategies for the management of metastatic bone diseases have been shifted to delay worsening of skeletal pain and aggravation of metastatic bone diseases. Bone modifying agents, such as bisophosphonate and human RANKL antibody, are considered as the standard of care for reducing SREs of patients with bone metastatic diseases. However, new therapeutic agents need to be developed to prolong the survival of patients with bone metastatic diseases.

The process of metastasis is so inefficient that only a small subset of tumor cells that leave the primary site can successfully navigate the process of metastasis to form clinical metastases in the bone. Understanding the biology of the successful metastatic cell, which has some of the characteristics of the theoretical cancer stem cell in the bone microenvironment, should provide the opportunity of addressing specific issues such as tumor dormancy, and drug resistance. New treatment of bone metastatic diseases could be accomplished by the combination of bone modifying agents to prevent SREs and agents targeting homeostatic factors that preserve survival, growth of the tumor cells in the bone microenvironment.

Our understanding on the molecular and cellular interactions in the bone microenvironment is significantly improving and the development of effective therapies for bone metastasis is becoming even more realistic.

Disclosure statement

The authors have declared that no conflict of interest exists.

Acknowledgments

The authors would like to express gratitude to Dr. David B. Alexander, in Nanotoxicology Project, Nagoya City University, Nagoya, Japan, for discussion and comments on the manuscript. This work was supported in part by a research grant from the Scientific Support Programs for Cancer Research Grant-in-Aid for Scientific Research on Innovative Areas (221S0001) from Ministry of Education, Culture, Sports, Science, and Technology, and a grant-in-aid for Scientific Research (C, 15K06837) from the Japan Society for the Promotion of Science.

References

[1] I.J. Fidler, The pathogenesis of cancer metastasis: the 'seed and soil' hypothesis revisited, Nat. Rev. Cancer 3 (2003) 453–458.
[2] I.J. Fidler, Critical factors in the biology of human cancer metastasis, Am. Surg. 61 (1995) 1065–1066.
[3] V. Montel, T.Y. Huang, E. Mose, K. Pestonjamasp, D. Tarin, Expression profiling of primary tumors and matched lymphatic and lung metastases in a xenogeneic breast cancer model, Am. J. Pathol. 166 (2005) 1565–1579.
[4] T.P. Butler, P.M. Gullino, Quantitation of cell shedding into efferent blood of mammary adenocarcinoma, Cancer Res. 35 (1975) 512–516.
[5] I.J. Fidler, M.L. Kripke, Metastasis results from preexisting variant cells within a malignant tumor, Science 197 (1977) 893–895.
[6] I.J. Fidler, Metastasis: quantitative analysis of distribution and fate of tumor emboli labeled with 125 I-5-iodo-2′-deoxyuridine, J. Natl. Cancer Inst. 45 (1970) 773–782.
[7] I.J. Fidler, Biological behavior of malignant melanoma cells correlated to their survival *in vivo*, Cancer Res. 35 (1975) 218–224.
[8] G.R. Mundy, Metastasis to bone: causes, consequences and therapeutic opportunities, Nat. Rev. Cancer 2 (2002) 584–593.
[9] T.A. Guise, K.S. Mohammad, G. Clines, E.G. Stebbins, D.H. Wong, L.S. Higgins, R. Vessella, E. Corey, S. Padalecki, L. Suva, J.M. Chirgwin, Basic mechanisms responsible for osteolytic and osteoblastic bone metastases, Clin. Cancer Res. 12 (2006) 6213s–6216s.
[10] S.A. Charhon, M.C. Chapuy, E.E. Delvin, A. Valentin-Opran, C.M. Edouard, P.J. Meunier, Histomorphometric analysis of sclerotic bone metastases from prostatic carcinoma special reference to osteomalacia, Cancer 51 (1983) 918–924.
[11] A. Leibbrandt, J.M. Penninger, RANKL/RANK as key factors for osteoclast development and bone loss in arthropathies, Adv. Exp. Med. Biol. 649 (2009) 100–113.
[12] J.M. Delaisse, T.L. Andersen, M.T. Engsig, K. Henriksen, T. Troen, L. Blavier, Matrix metalloproteinases (MMP) and cathepsin K contribute differently to osteoclastic activities, Microsc. Res. Tech. 61 (2003) 504–513.
[13] B. Guo, D.J. Villeneuve, S.L. Hembruff, A.F. Kirwan, D.E. Blais, M. Bonin, A.M. Parissenti, Cross-resistance studies of isogenic drug-resistant breast tumor cell lines support recent clinical evidence suggesting that sensitivity to paclitaxel may be strongly compromised by prior doxorubicin exposure, Breast Cancer Res. Treat. 85 (2004) 31–51.
[14] Y. Kang, P.M. Siegel, W. Shu, M. Drobnjak, S.M. Kakonen, C. Cordon-Cardo, T.A. Guise, J. Massague, A multigenic program mediating breast cancer metastasis to bone, Cancer Cell 3 (2003) 537–549.
[15] C. Kuperwasser, S. Dessain, B.E. Bierbaum, D. Garnet, K. Sperandio, G.P. Gauvin, S.P. Naber, R.A. Weinberg, M. Rosenblatt, A mouse model of human breast cancer metastasis to human bone, Cancer Res. 65 (2005) 6130–6138.
[16] B.O. Murphy, S. Joshi, A. Kessinger, E. Reed, J.G. Sharp, A murine model of bone marrow micrometastasis in breast cancer, Clin. Exp. Metastasis 19 (2002) 561–569.
[17] J.A. Nemeth, J.F. Harb, U. Barroso Jr., Z. He, D.J. Grignon, M.L. Cher, Severe combined immunodeficient-hu model of human prostate cancer metastasis to human bone, Cancer Res. 59 (1999) 1987–1993.
[18] A.H. Reddi, D. Roodman, C. Freeman, S. Mohla, Mechanisms of tumor metastasis to the bone: challenges and opportunities, J. Bone Miner. Res. 18 (2003) 190–194.
[19] E. Shtivelman, R. Namikawa, Species-specific metastasis of human tumor cells in the severe combined immunodeficiency mouse engrafted with human tissue, Proc. Natl. Acad. Sci. U. S. A. 92 (1995) 4661–4665.
[20] S. Paget, The distribution of secondary growths in cancer of the breast. 1889, Cancer Metastasis Rev. 8 (1989) 98–101.
[21] S.A. Patel, M.A. Dave, R.G. Murthy, K.Y. Helmy, P. Rameshwar, Metastatic breast cancer cells in the bone marrow microenvironment: novel insights into oncoprotection, Oncol. Rev. 5 (2011) 93–102.
[22] V.A. Siclari, T.A. Guise, J.M. Chirgwin, Molecular interactions between breast cancer cells and the bone microenvironment drive skeletal metastases, Cancer Metastasis Rev. 25 (2006) 621–633.
[23] D. Luis-Ravelo, I. Anton, S. Vicent, I. Hernandez, K. Valencia, C. Zandueta, S. Martinez-Canarias, A. Gurpide, F. Lecanda, Tumor–stromal interactions of the bone microenvironment: *in vitro* findings and potential *in vivo* relevance in metastatic lung cancer models, Clin. Exp. Metastasis 28 (2011) 779–791.
[24] D.M. Sosnoski, V. Krishnan, W.J. Kraemer, C. Dunn-Lewis, A.M. Mastro, Changes in cytokines of the bone microenvironment during breast cancer metastasis, Int. J. Breast Cancer 2012 (2012) 160265.
[25] T. Yoneda, T. Hiraga, Crosstalk between cancer cells and bone microenvironment in bone metastasis, Biochem. Biophys. Res. Commun. 328 (2005) 679–687.
[26] T. Hiraga, A. Ueda, D. Tamura, K. Hata, F. Ikeda, P.J. Williams, T. Yoneda, Effects of oral UFT combined with or without zoledronic acid on bone metastasis in the 4T1/luc mouse breast cancer, Int. J. Cancer 106 (2003) 973–979.
[27] H. Iguchi, S. Tanaka, Y. Ozawa, T. Kashiwakuma, T. Kimura, T. Hiraga, H. Ozawa, A. Kono, An experimental model of bone metastasis by human lung cancer cells: the role of parathyroid hormone-related protein in bone metastasis, Cancer Res. 56 (1996) 4040–4043.
[28] C.C. Lynch, A. Hikosaka, H.B. Acuff, M.D. Martin, N. Kawai, R.K. Singh, T.C. Vargo-Gogola, J.L. Begtrup, T.E. Peterson, B. Fingleton, T. Shirai, L.M. Matrisian, M. Futakuchi, MMP-7 promotes prostate cancer-induced osteolysis *via* the solubilization of RANKL, Cancer Cell 7 (2005) 485–496.
[29] M. Futakuchi, K.C. Nannuru, M.L. Varney, A. Sadanandam, K. Nakao, K. Asai, T. Shirai, S.Y. Sato, R.K. Singh, Transforming growth factor-beta signaling at the tumor-bone interface promotes mammary tumor growth and osteoclast activation, Cancer Sci. 100 (2009) 71–81.
[30] M. Futakuchi, R.K. Singh, Animal model for mammary tumor growth in the bone microenvironment, Breast Cancer (Tokyo, Jpn.) 20 (2013) 195–203.
[31] T.J. Wilson, K.C. Nannuru, M. Futakuchi, R.K. Singh, Cathepsin G-mediated enhanced TGF-beta signaling promotes angiogenesis *via* upregulation of VEGF and MCP-1, Cancer Lett. 288 (2010) 162–169.
[32] A. Sadanandam, M. Futakuchi, C.A. Lyssiotis, W.J. Gibb, R.K. Singh, A cross-species analysis of a mouse model of breast cancer-specific osteolysis and human bone metastases using gene expression profiling, BMC Cancer 11 (2011) 304.
[33] T. Ohshiba, C. Miyaura, M. Inada, A. Ito, Role of RANKL-induced osteoclast formation and MMP-dependent matrix degradation in bone destruction by breast cancer metastasis, Br. J. Cancer 88 (2003) 1318–1326.
[34] E. Jimi, K. Aoki, H. Saito, F. D'Acquisto, M.J. May, I. Nakamura, T. Sudo, T. Kojima, F. Okamoto, H. Fukushima, K. Okabe, K. Ohya, S. Ghosh, Selective inhibition of NF-kappa B blocks osteoclastogenesis and prevents inflammatory bone destruction *in vivo*, Nat. Med. 10 (2004) 617–624.
[35] T.J. Wilson, K.C. Nannuru, M. Futakuchi, A. Sadanandam, R.K. Singh, Cathepsin G enhances mammary tumor-induced osteolysis by generating soluble receptor activator of nuclear factor-kappaB ligand, Cancer Res. 68 (2008) 5803–5811.
[36] J.E. Fata, Y.Y. Kong, J. Li, T. Sasaki, J. Irie-Sasaki, R.A. Moorehead, R. Elliott, S. Scully, E.B. Voura, D.L. Lacey, W.J. Boyle, R. Khokha, J.M. Penninger, The osteoclast differentiation factor osteoprotegerin-ligand is essential for mammary gland development, Cell 103 (2000) 41–50.

[37] Y. Cao, G. Bonizzi, T.N. Seagroves, F.R. Greten, R. Johnson, E.V. Schmidt, M. Karin, IKKalpha provides an essential link between RANK signaling and cyclin D1 expression during mammary gland development, Cell 107 (2001) 763–775.
[38] Y. Cao, J.L. Luo, M. Karin, IkappaB kinase alpha kinase activity is required for self-renewal of ErbB2/Her2-transformed mammary tumor-initiating cells, Proc. Natl. Acad. Sci. U. S. A. 104 (2007) 15852–15857.
[39] J.L. Luo, W. Tan, J.M. Ricono, O. Korchynskyi, M. Zhang, S.L. Gonias, D.A. Cheresh, M. Karin, Nuclear cytokine-activated IKKalpha controls prostate cancer metastasis by repressing Maspin, Nature 446 (2007) 690–694.
[40] W. Tan, W. Zhang, A. Strasner, S. Grivennikov, J.Q. Cheng, R.M. Hoffman, M. Karin, Tumour-infiltrating regulatory T cells stimulate mammary cancer metastasis through RANKL–RANK signalling, Nature 470 (2011) 548–553.
[41] R.E. Coleman, Future directions in the treatment and prevention of bone metastases, Am. J. Clin. Oncol. 25 (2002) S32–S38.
[42] R.E. Coleman, Clinical features of metastatic bone disease and risk of skeletal morbidity, Clin. Cancer Res. 12 (2006) 6243s–6249s.
[43] R.E. Coleman, R.D. Rubens, The clinical course of bone metastases from breast cancer, Br. J. Cancer 55 (1987) 61–66.
[44] C. Clare, D. Royle, K. Saharia, H. Pearse, S. Oxberry, K. Oakley, L. Allsopp, A.S. Rigby, M.J. Johnson, Painful bone metastases: a prospective observational cohort study, Palliat. Med. 19 (2005) 521–525.
[45] C.S. Cleeland, The measurement of pain from metastatic bone disease: capturing the patient's experience, Clin. Cancer Res. 12 (2006) 6236s–6242s.
[46] D.H. Henry, L. Costa, F. Goldwasser, V. Hirsh, V. Hungria, J. Prausova, G.V. Scagliotti, H. Sleeboom, A. Spencer, S. Vadhan-Raj, R. von Moos, W. Willenbacher, P.J. Woll, J. Wang, Q. Jiang, S. Jun, R. Dansey, H. Yeh, Randomized, double-blind study of denosumab *versus* zoledronic acid in the treatment of bone metastases in patients with advanced cancer (excluding breast and prostate cancer) or multiple myeloma, J. Clin. Oncol. 29 (2011) 1125–1132.
[47] W. Leppert, Pain management in patients with cancer: focus on opioid analgesics, Curr. Pain Headache Rep. 15 (2011) 271–279.
[48] A. Vainio, A. Auvinen, Prevalence of symptoms among patients with advanced cancer: an international collaborative study. Symptom Prevalence Group, J. Pain Symptom Manag. 12 (1996) 3–10.
[49] J.A. Dewar, Managing Metastatic Bone Pain, 2004.
[50] C.H. Van Poznak, S. Temin, G.C. Yee, N.A. Janjan, W.E. Barlow, J.S. Biermann, L.D. Bosserman, C. Geoghegan, B.E. Hillner, R.L. Theriault, D.S. Zuckerman, J.H. Von Roenn, O., American Society of Clinical Oncology executive summary of the clinical practice guideline update on the role of bone-modifying agents in metastatic breast cancer, J. Clin. Oncol. 29 (2011) 1221–1227.
[51] M.R. Smith, F. Saad, S. Oudard, N. Shore, K. Fizazi, P. Sieber, B. Tombal, R. Damiao, G. Marx, K. Miller, P. Van Veldhuizen, J. Morote, Z. Ye, R. Dansey, C. Goessl, Denosumab and bone metastasis-free survival in men with nonmetastatic castration-resistant prostate cancer: exploratory analyses by baseline prostate-specific antigen doubling time, J. Clin. Oncol. 31 (2013) 3800–3806.
[52] M.R. Smith, F. Saad, R. Coleman, N. Shore, K. Fizazi, B. Tombal, K. Miller, P. Sieber, L. Karsh, R. Damiao, T.L. Tammela, B. Egerdie, H. Van Poppel, J. Chin, J. Morote, F. Gomez-Veiga, T. Borkowski, Z. Ye, A. Kupic, R. Dansey, C. Goessl, Denosumab and bone-metastasis-free survival in men with castration-resistant prostate cancer: results of a phase 3, randomised, placebo-controlled trial, Lancet 379 (2012) 39–46.
[53] D.A. Berry, Biomarker studies and other difficult inferential problems: statistical caveats, Semin. Oncol. 34 (2007) S17–S22.
[54] I.P. Garraway, Targeting the RANKL pathway: putting the brakes on prostate cancer progression in bone, J. Clin. Oncol. 31 (2013) 3838–3840.
[55] F. Saad, J. Eastham, Zoledronic acid improves clinical outcomes when administered before onset of bone pain in patients with prostate cancer, Urology 76 (2010) 1175–1181.
[56] F. Saad, D.M. Gleason, R. Murray, S. Tchekmedyian, P. Venner, L. Lacombe, J.L. Chin, J.J. Vinholes, J.A. Goas, M. Zheng, Long-term efficacy of zoledronic acid for the prevention of skeletal complications in patients with metastatic hormone-refractory prostate cancer, J. Natl. Cancer Inst. 96 (2004) 879–882.
[57] B.E. Hillner, J.N. Ingle, J.R. Berenson, N.A. Janjan, K.S. Albain, A. Lipton, G. Yee, J.S. Biermann, R.T. Chlebowski, D.G. Pfister, American Society of Clinical Oncology guideline on the role of bisphosphonates in breast cancer. American Society of Clinical Oncology Bisphosphonates Expert Panel, J. Clin. Oncol. 18 (2000) 1378–1391.
[58] B.E. Hillner, J.N. Ingle, R.T. Chlebowski, J. Gralow, G.C. Yee, N.A. Janjan, J.A. Cauley, B.A. Blumenstein, K.S. Albain, A. Lipton, S. Brown, American Society of Clinical Oncology 2003 update on the role of bisphosphonates and bone health issues in women with breast cancer, J. Clin. Oncol. 21 (2003) 4042–4057.
[59] R. von Moos, F. Strasser, S. Gillessen, K. Zaugg, Metastatic bone pain: treatment options with an emphasis on bisphosphonates, Support. Care Cancer 16 (2008) 1105–1115.
[60] C.A. O'Brien, A. Pollett, S. Gallinger, J.E. Dick, A human colon cancer cell capable of initiating tumour growth in immunodeficient mice, Nature 445 (2007) 106–110.
[61] L. Ricci-Vitiani, D.G. Lombardi, E. Pilozzi, M. Biffoni, M. Todaro, C. Peschle, R. De Maria, Identification and expansion of human colon-cancer-initiating cells, Nature 445 (2007) 111–115.
[62] M.E. Prince, R. Sivanandan, A. Kaczorowski, G.T. Wolf, M.J. Kaplan, P. Dalerba, I.L. Weissman, M.F. Clarke, L.E. Ailles, Identification of a subpopulation of cells with cancer stem cell properties in head and neck squamous cell carcinoma, Proc. Natl. Acad. Sci. U. S. A. 104 (2007) 973–978.
[63] T. Schatton, G.F. Murphy, N.Y. Frank, K. Yamaura, A.M. Waaga-Gasser, M. Gasser, Q. Zhan, S. Jordan, L.M. Duncan, C. Weishaupt, R.C. Fuhlbrigge, T.S. Kupper, M.H. Sayegh, M.H. Frank, Identification of cells initiating human melanomas, Nature 451 (2008) 345–349.
[64] A. Eramo, F. Lotti, G. Sette, E. Pilozzi, M. Biffoni, A. Di Virgilio, C. Conticello, L. Ruco, C. Peschle, R. De Maria, Identification and expansion of the tumorigenic lung cancer stem cell population, Cell Death Differ. 15 (2008) 504–514.
[65] Z.F. Yang, D.W. Ho, M.N. Ng, C.K. Lau, W.C. Yu, P. Ngai, P.W. Chu, C.T. Lam, R.T. Poon, S.T. Fan, Significance of CD90+ cancer stem cells in human liver cancer, Cancer Cell 13 (2008) 153–166.
[66] S.K. Singh, C. Hawkins, I.D. Clarke, J.A. Squire, J. Bayani, T. Hide, R.M. Henkelman, M.D. Cusimano, P.B. Dirks, Identification of human brain tumour initiating cells, Nature 432 (2004) 396–401.
[67] M.D. Curley, V.A. Therrien, C.L. Cummings, P.A. Sergent, C.R. Koulouris, A.M. Friel, D.J. Roberts, M.V. Seiden, D.T. Scadden, B.R. Rueda, R. Foster, CD133 expression defines a tumor initiating cell population in primary human ovarian cancer, Stem Cells 27 (2009) 2875–2883.
[68] A.T. Collins, P.A. Berry, C. Hyde, M.J. Stower, N.J. Maitland, Prospective identification of tumorigenic prostate cancer stem cells, Cancer Res. 65 (2005) 10946–10951.
[69] M. Al-Hajj, M.S. Wicha, A. Benito-Hernandez, S.J. Morrison, M.F. Clarke, Prospective identification of tumorigenic breast cancer cells, Proc. Natl. Acad. Sci. U. S. A. 100 (2003) 3983–3988.
[70] R. Adikrisna, S. Tanaka, S. Muramatsu, A. Aihara, D. Ban, T. Ochiai, T. Irie, A. Kudo, N. Nakamura, S. Yamaoka, S. Arii, Identification of pancreatic cancer stem cells and selective toxicity of chemotherapeutic agents, Gastroenterology 143 (2012) 234–245 (e237).
[71] P.C. Hermann, S.L. Huber, T. Herrler, A. Aicher, J.W. Ellwart, M. Guba, C.J. Bruns, C. Heeschen, Distinct populations of cancer stem cells determine tumor growth and metastatic activity in human pancreatic cancer, Cell Stem Cell 1 (2007) 313–323.
[72] C. Li, D.G. Heidt, P. Dalerba, C.F. Burant, L. Zhang, V. Adsay, M. Wicha, M.F. Clarke, D.M. Simeone, Identification of pancreatic cancer stem cells, Cancer Res. 67 (2007) 1030–1037.
[73] Y. Shiozawa, A.M. Havens, K.J. Pienta, R.S. Taichman, The bone marrow niche: habitat to hematopoietic and mesenchymal stem cells, and unwitting host to molecular parasites, Leukemia 22 (2008) 941–950.
[74] T. Sugiyama, H. Kohara, M. Noda, T. Nagasawa, Maintenance of the hematopoietic stem cell pool by CXCL12-CXCR4 chemokine signaling in bone marrow stromal cell niches, Immunity 25 (2006) 977–988.
[75] R.S. Taichman, M.J. Reilly, S.G. Emerson, Human osteoblasts support human hematopoietic progenitor cells *in vitro* bone marrow cultures, Blood 87 (1996) 518–524.
[76] D.N. Haylock, S.K. Nilsson, Stem cell regulation by the hematopoietic stem cell niche, Cell Cycle 4 (2005) 1353–1355.
[77] R.S. Taichman, Blood and bone: two tissues whose fates are intertwined to create the hematopoietic stem-cell niche, Blood 105 (2005) 2631–2639.
[78] J. Zhu, S.G. Emerson, A new bone to pick: osteoblasts and the haematopoietic stem-cell niche, Bioessays 26 (2004) 595–599.
[79] R.N. Kaplan, R.D. Riba, S. Zacharoulis, A.H. Bramley, L. Vincent, C. Costa, D.D. MacDonald, D.K. Jin, K. Shido, S.A. Kerns, Z. Zhu, D. Hicklin, Y. Wu, J.L. Port, N. Altorki, E.R. Port, D. Ruggero, S.V. Shmelkov, K.K. Jensen, S. Rafii, D. Lyden, VEGFR1-positive haematopoietic bone marrow progenitors initiate the pre-metastatic niche, Nature 438 (2005) 820–827.
[80] L.L. Campbell, K. Polyak, Breast tumor heterogeneity: cancer stem cells or clonal evolution? Cell Cycle 6 (2007) 2332–2338.
[81] M.F. Clarke, J.E. Dick, P.B. Dirks, C.J. Eaves, C.H. Jamieson, D.L. Jones, J. Visvader, I.L. Weissman, G.M. Wahl, Cancer stem cells—perspectives on current status and future directions: AACR workshop on cancer stem cells, Cancer Res. 66 (2006) 9339–9344.
[82] S.A. Stacker, M.E. Baldwin, M.G. Achen, The role of tumor lymphangiogenesis in metastatic spread, FASEB J. 16 (2002) 922–934.
[83] S.S. Sundar, T.S. Ganesan, Role of lymphangiogenesis in cancer, J. Clin. Oncol. 25 (2007) 4298–4307.
[84] I. Van der Auwera, Y. Cao, J.C. Tille, M.S. Pepper, D.G. Jackson, S.B. Fox, A.L. Harris, L.Y. Dirix, P.B. Vermeulen, First international consensus on the methodology of lymphangiogenesis quantification in solid human tumours, Br. J. Cancer 95 (2006) 1611–1625.
[85] F. Li, B. Tiede, J. Massague, Y. Kang, Beyond tumorigenesis: cancer stem cells in metastasis, Cell Res. 17 (2007) 3–14.

Microbiology and Immunology

Microbiol Immunol 2016; 60: 35–46
doi: 10.1111/1348-0421.12338

ORIGINAL ARTICLE

C5a inhibitor protects against ischemia/reperfusion injury in rat small intestine

Eszter Tuboly[1], Mitsuru Futakuchi[2], Gabriella Varga[1], Daniel Érces[1], Tünde Tőkés[1], Andras Mészáros[1], József Kaszaki[1], Masumi Suzui[2], Masaki Imai[3], Alan Okada[4], Noriko Okada[5], Mihály Boros[1] and Hidechika Okada[5,*]

[1]Institute of Surgical Research, Faculty of Medicine, University of Szeged, 6 Szőkefalvi-Nagy Béla Street, Szeged, 6720, Hungary, [2]Department of Molecular Toxicology, [3]Department of Immunology, Graduate School of Medical Sciences, Nagoya City University, 1-Kawasumi, Mizuho-cho, Mizuho-ku, Nagoya, 467-8601, [4]Research Institute for Protein Science, 2-18 Nakayama-cho, Mizuho-ku, Nagoya, 467-0803, Japan and [5]Professor Emeritus, Nagoya City University

ABSTRACT

Acute mesenteric ischemia (AMI) is caused by considerable intestinal injury, which is associated with intestinal ischemia followed by reperfusion. To elucidate the mechanisms of ischemia/reperfusion injuries, a C5a inhibitory peptide termed AcPepA was used to examine the role of C5a anaphylatoxin, induction of inflammatory cells, and cell proliferation of the intestinal epithelial cells in an experimental AMI model. In this rat model, the superior mesenteric artery was occluded and subsequently reperfused (Induce-I/R). Other groups were treated with AcPepA before ischemia or reperfusion. Induce-I/R induced injuries in the intestine and AcPepA significantly decreased the proportion of severely injured villi. Induce-I/R induced secondary receptor for C5a-positive polymorphonuclear leukocytes in the vessels and CD204-positive macrophages near the injured site; this was correlated with hypoxia-induced factor 1-alpha-positive cells. Induction of these inflammatory cells was attenuated by AcPepA. In addition, AcPepA increased proliferation of epithelial cells in the villi, possibly preventing further damage. Therefore, Induce-I/R activates C5a followed by the accumulation of polymorphonuclear leukocyte and hypoxia-induced factor 1-alpha-producing macrophages, leading to villus injury. AcPepA, a C5a inhibitory peptide, blocks the deleterious effects of C5a, indicating it has a therapeutic effect on the inflammatory consequences of experimental AMI.

Key words complement C5a, hypoxia-induced factor 1-alpha, ischemia, macrophage.

Acute mesenteric ischemia, a critical circulatory condition, is caused by an arterial or venous thrombosis or embolism (1, 2). The overall mortality rate of AMI has remained at 60% to 80% over the last 25 years and the incidence of this disease is increasing (3, 4). AMI comprises a group of pathologic processes that have a common end point—intestinal necrosis (4). The intestinal epithelium is probably one of the most sensitive tissues to I/R injury in the body (5); intestinal ischemia rapidly progresses to severe metabolic derangements, infiltration of inflammatory cells, loss of villi and epithelial cells, and mucosal destruction, culminating in irreversible bowel necrosis (3).

Reoxygenation is crucial for cell survival, however, it has been well established that I/R causes much more

Correspondence
Mitsuru Futakuchi, Department of Molecular Toxicology, Graduate School of Medical Sciences, Nagoya City University, 1-Kawasumi, Mizuho-cho, Mizuho-ku, Nagoya, 467-8601, Japan. Tel:+81-52-853-8992, fax: +81-52-853-8996; email: futakuch@med.nagoya-cu.ac.jp

*Present address: Research Institute for Protein Science, Nakayama-cho 2-18, Mizuho-ku, Nagoya 467-0803, Japan

Received 9 November 2015; accepted 11 November 2015.

List of Abbreviations: AMI, acute mesenteric ischemia; C5L2, secondary receptor for C5a; CD68+MAC, CD68-positive macrophage; CD204+MAC, CD204-positive macrophage; HIF-1α, hypoxia-induced factor 1-alpha; IHC, immunohistochemical staining; I/R, Intestinal ischemia followed by reperfusion; Induce-I/R, induction of intestinal ischemia; Induce-I/R, induction of intestinal ischemia followed by reperfusion; PCNA, proliferating cell nuclear antigen; PMN, polymorphonuclear leukocyte.

severe tissue injury than that induced by ischemia alone (6). Investigation of the development of I/R damage has revealed significant regeneration of the mucosa, which parallels necrosis and apoptosis of the epithelial cells of the villi (7, 8). Published studies have suggested that I/R injury involves multiple processes, including activation of inflammatory cells with cytokine production followed by decay or regeneration of the injured epithelial cells. A variety of endogenous compounds and effector cells have been identified as mediators of I/R injury, including platelet-activating factor (9), TNF-α (10), IL-6 (11) and oxygen radicals (12). It is also well-known that I/R induces the so-called antigen-independent inflammatory pathway via which cellular and molecular participants of the immune system can be activated (13).

The complement system has been implicated as a major candidate in I/R injury, several studies having suggested that complement activation is involved in I/R injury in the gut (14–16). Complement activation results in production of C5a, which has been shown to be fundamental in exacerbation of I/R injuries (17). Complement activation occurs in the early stages of inflammation. In the case of gut I/R, activated complement induces activation of inflammatory cells, such as PMNs and macrophages, which have been demonstrated to play central roles in the development of I/R injury (18–20). In addition, C5a has been demonstrated to enhance the release of a number of pro-inflammatory cytokines from activated PMNs and macrophages (21–23). Furthermore, inhibition of C5a by a complementary peptide to C5a (AcPepA) reportedly suppresses the release of high mobility group box 1 resulting in rescue of monkeys injected with lethal doses of LPS (24).

C5a is considered to be a major factor in complement-mediated I/R tissue injury. Thus, the development of I/R injury involves multiple processes, such as C5a generation, induction of inflammatory cells and cytokine production, all of which lead to apoptosis and regeneration of the injured intestinal epithelial cells. These processes would involve cellular and molecular cross-talk among inflammatory cells, which has not yet been investigated in detail. C5a is believed to be a major factor in complement-mediated I/R tissue injury. Accordingly, the present study aimed to shed more light on the possible cellular and molecular pathways involved in the proliferative consequences of I/R events.

To this end we used AcPepA, which we have generated as an inhibitory complementary peptide (C-peps) of C5a (25–27) and examined its modulating effects on certain inflammatory responses, such as induction of C5L2-positive cells, induction of activated macrophages and involvement of HIF1-α in I/R injury, in a clinically relevant animal model of AMI.

MATERIALS AND METHODS

Animals and surgical preparation

The experiments were performed in full accordance with the National Institutes of Health guidelines on the handling and care of experimental animals and the study was approved by the Animal Welfare Committee of the University of Szeged.

A total of 35 male Sprague–Dawley rats (250–350 g body weight) were anesthetized with sodium pentobarbital (50 mg/kg, intraperitoneally) and placed in a supine position on a heating pad. Tracheostomy was performed to facilitate spontaneous breathing, after which the right jugular vein was cannulated with PE50 tubing for administration of Ringer's lactate infusion (10 mL/kg/hr) and to facilitate maintenance of anesthesia with sodium pentobarbital throughout the experiment.

The right common carotid artery was cannulated to measure the mean arterial pressure, which was measured at 30-min intervals and monitored throughout the investigation. The i.v. administration of AcPepA did not influence the mean arterial pressure of any of the treated animals (data not shown).

Experimental protocol

After confirming cardiovascular stabilization during the 30-minute recovery from anesthesia, a median laparotomy was performed to carry out the following experimental protocol. The animals were divided into five groups. Rats in group A served as a sham-operated group ($n = 5$). Rats in groups B ($n = 8$) and C ($n = 8$), were exposed to ischemic insult, in which the superior mesenteric artery was occluded for 45 min with an atraumatic vascular clamp (Induce-I). Rats in groups D ($n = 7$) and E ($n = 7$), were subjected to ischemia followed by reperfusion for 30 min (Induce-I/R). Rats in groups C and E were given AcPepA (courtesy of Alan Okada, Research Institute for Protein Science, Nagoya, Japan) (4 mg/kg iv. in Ringer's lactate solution) 30 min after initiation of ischemia. The tissue samples were divided into two portions. One was used for histological and immunohistochemical analyses, whereas the other served as materials for proteomic investigation and was stored at −70°C. For histology, samples were fixed with 4% paraformaldehyde and then embedded and processed for further analysis. The fixed tissue was attached to hard backing with staples to ensure the optimal longitudinal orientation of the section.

Evaluation of the degree of injury to the villi

To evaluate the effects of ischemia, I/R and AcPepA treatment on small intestinal villi, the percentage of injured villi was calculated for each animal. The total number of villi in each hematoxylin and eosin-stained section was counted (20–25 fields at 400× magnification). Each villus was assigned to one of four categories (uninjured, slight, moderate or severe), depending on the degree of damage (length of the villus, infiltration of inflammatory cells, presence of surface erosion and amount of necrotic epithelium in the lumen).

In vivo detection of structural damage

The extent of microvascular and epithelial damage in the terminal ileum was evaluated by fluorescence real-time laser scanning confocal endomicroscopy (Five1, Ex. 488 nm, Em. 505–585 nm; Optiscan, Melbourne, Victoria, Australia) 30 min after the beginning of reperfusion. The mucosal surface of the terminal ileum was surgically exposed 5 cm proximal to the cecum and laid flat for examination. The microvascular structure was recorded after i.v. administration of 0.3 mL of fluorescein isothiocyanate-dextran (150 kDa, Sigma-Aldrich, St. Louis, Missouri, USA, 20 mg mL^{-1} solution dissolved in physiological saline). Confocal imaging was performed 5 min after dye administration (one scan/image, 1024 × 512 pixels and 475 × 475 μm per image). The villous architecture was examined following topical application of the fluorescent dye acridine orange (Sigma-Aldrich), surplus dye being flushed away from the mucosal surface of the ileum with physiological saline 2 min before imaging.

Immunohistochemical analysis

CD68 receptor, PCNA, C5L2 and CD204 receptors and HIF-1α expression were evaluated by IHC of sections of the small intestine. For this IHC study, the following diluted primary antibodies were prepared: PCNA (Clone PC10, 1:500; Dako Japan., Tokyo, Japan), C5L2 (1:100; kindly provided by Masaki Imai, Department of Immunology, Nagoya City University, Nagoya, Japan), CD68 primary antibody (1:100; BMA Biomedicals, Augst, Switzerland), CD204 (1:100; Trans Genic, Kumamoto, Japan), and HIF1-α (1:100; Thermo Fisher Scientific, Cheshire, UK). The entire IHC investigation was carried out using an automatic IHC machine, Leica Bond-max (Leica Microsystems, Tokyo, Japan) according to the manufacturer's instructions. For quantitative analysis, immunostained sections were examined under a light microscope, and the numbers of nuclei and cells positive for PCNA, C5L2, CD68, CD204 and HIF1-α enumerated at a magnification of ×400 for each region of the normal and injured villi, respectively.

Statistical analysis

Statistical analysis of the *in vivo* data was performed using Kruskal–Wallis and Bonferroni/Dunn multiple comparison tests. Data are presented as means ± SD. Values of $P < 0.05$ were deemed significant.

RESULTS

Effect of AcPepA on the degree of small intestinal injury

Induce-I and Induce-I/R induced various degrees of injury to the small intestine. The villi were sorted into four categories: uninjured (Fig. 1a), slightly (Fig. 1b), moderately (Fig. 1c) and severely injured (Fig. 1d), based on various histological criteria. About 96% of the intestinal villi in the control group were classified as uninjured (Table 1). The degrees of injury to the villi induced by Induce-I and Induce-I/R are shown in Table 1. The proportion of severely injured villi in the Induce-I/R group (76%) was significantly higher than that in the Induce-I group (6%) and was significantly reduced by AcPepA administration (to 24%; Table 1, Figure 1e).

Because Induce-I/R caused more severe injury to the small intestinal epithelium (76%) than did Induce-I (6%), the surface and micro-vessels of the small intestinal villi were further examined by confocal laser scanning endomicroscopy. Acridine orange staining revealed that the surfaces of the villi in the control group were smooth (Fig. 1f). Although longitudinal fissures and epithelial gaps filled with tissue debris were observed in the Induce-I/R group (Fig. 1g), only a few shed cells and epithelial gaps were observed in the AcPepA administration following Induce-I/R group (Figure 1h). Similarly, microvessel structures observed in the control group (Fig. 1i) were disorganized and fluorescent dye leakage was recorded in several areas of small intestinal villi (Fig. 1j). The extent of leakage was diminished by AcPepA administration following Induce-I/R (Fig. 1k). Thus, AcPepA treatment significantly reduced the degree of microvascular damage and preserved the epithelial morphology.

Taken together, these results suggest that Induce-I/R causes more severe injury to the small intestinal epithelium than does Treat-I alone, indicating that C5a activation may be involved in the increased damage that can be suppressed by the C5a-inhibitory peptide AcPepA.